

PL-TR-96-2075

TRANSPORTABLE TIME DOMAIN DISCRIMINANTS

**Donald V. Helmberger
Lupei Zhu
Larry Burdick**

**California Institute of Technology
1200 E. California Blvd
Pasadena, CA 91125**

23 August 1996

DTIC QUALITY INSPECTED 2

**Final Report
15 June 1995-14 June 1996**

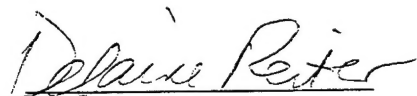
APPROVED FOR PUBLIC RELEASE; DISTRIBUTION UNLIMITED



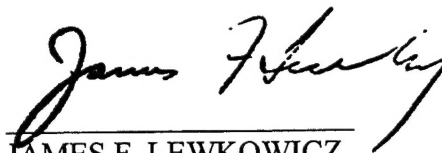
**PHILLIPS LABORATORY
Directorate of Geophysics
AIR FORCE MATERIEL COMMAND
HANSCom AFB, MA 01731-3010**

19970206 109

"This technical report has been reviewed and is approved for publication."



DELAINE REITER
Contract Manager
Earth Sciences Division



JAMES F. LEWKOWICZ
Director
Earth Sciences Division

This report has been reviewed by the ESD Public Affairs Office (PA) and is releasable to the National Technical Information Service (NTIS).

Qualified requestors may obtain copies from the Defense Technical Information Center. All others should apply to the National Technical Information Service.

If your address has changed, or you wish to be removed from the mailing list, or if the addressee is no longer employed by your organization, please notify PL/IM, 29 Randolph Road, Hanscom AFB, MA 01731-3010. This will assist us in maintaining a current mailing list.

Do not return copies of this report unless contractual obligations or notices on a specific document requires that it be returned.

REPORT DOCUMENTATION PAGE			Form Approved OMB No. 0704-0188	
<small>Public reporting burden for this collection of information is estimated to average 1 hour per response, including the time for reviewing instructions, searching existing data sources, gathering and maintaining the data needed, and completing and reviewing the collection of information. Send comments regarding this burden estimate or any other aspect of this collection of information, including suggestions for reducing this burden, to Washington Headquarters Services, Directorate for Information Operations and Reports, 1215 Jefferson Davis Highway, Suite 1204, Arlington, VA 22202-4302, and to the Office of Management and Budget, Paperwork Reduction Project (0704-0188), Washington, DC 20503.</small>				
1. AGENCY USE ONLY (Leave blank)	2. REPORT DATE 23 August 1996	3. REPORT TYPE AND DATES COVERED Final - 15 June 1995-14 June 1996		
4. TITLE AND SUBTITLE Transportable Time Domain Discriminants		5. FUNDING NUMBERS F19628-95-C-0095 PE 62101F PR7600 TRGM WUAD		
6. AUTHOR(S) Don V. Helmberger, Lupei Zhu, and Larry Burdick				
7. PERFORMING ORGANIZATION NAME(S) AND ADDRESS(ES) California Institute of Technology 1200 E. California Blvd. Pasadena, California 91125		8. PERFORMING ORGANIZATION REPORT NUMBER		
9. SPONSORING / MONITORING AGENCY NAME(S) AND ADDRESS(ES) Phillips Laboratory 29 Randolph Road Hanscom AFB, MA 01731-3010 Contract Manager: Dr. Delaine Reiter/GPE		10. SPONSORING / MONITORING AGENCY REPORT NUMBER PL-TR-96-2075		
11. SUPPLEMENTARY NOTES				
12a. DISTRIBUTION / AVAILABILITY STATEMENT Approved for public release; distribution unlimited			12b. DISTRIBUTION CODE	
13. ABSTRACT (Maximum 200 words) We have examined broadband waveforms from a large number of NTS explosions and earthquakes throughout the southwestern United States in order to characterize seismic sources. Explosions were found to be richer in coda energy than earthquakes. Most earthquakes show relatively little long-period ($T > 4$ sec) coda energy and tend to be richer in long-period and shear-wave energy than explosions. We have developed several seismic discriminants based on these observations and our modeling experience. One promising discriminant is the ratio of short-period vertical components, P-wavetrain energy, to long-period surface wave energy, averaged over three components. Explosions tend to have a higher ratio than do earthquakes, essentially an extension of M_b/M_s . Magnitude threshold for this discriminant is about 3.5. Another useful discriminant is based on the total broadband energy to moment ratio where explosions are distinguished by their stronger energy levels relative to their long-period amplitudes. This approach requires Green's functions, a source estimator program, and processes all events as earthquakes. For this method to be effective requires the calibration of the region using relatively large earthquakes, $M > 5$, but does not require calibrations of explosions.				
14. SUBJECT TERMS NTS explosions, earthquakes, southwestern United States seismic sources, discriminants.			15. NUMBER OF PAGES 50	
			16. PRICE CODE	
17. SECURITY CLASSIFICATION OF REPORT Unclassified	18. SECURITY CLASSIFICATION OF THIS PAGE Unclassified	19. SECURITY CLASSIFICATION OF ABSTRACT Unclassified	20. LIMITATION OF ABSTRACT Unlimited	

Table of Contents

Abstract

1. Introduction
2. Estimation of Earthquake Parameters
3. Source Estimation Using True Amplitude Waveforms
4. Focal Depth Distribution and the Seismogenic Zone in Southern California
5. Estimation of Seismic Energy and Discriminants
6. Discussion
7. Acknowledgments
8. References

Illustrations

1. Map displaying the TERRAscope stations as triangles and focal mechanisms of the 335 local earthquakes, $M_L > 3.5$, as determined by waveform inversion.
2. Comparison of the vertical motions produced by two earthquakes (Skull Mtn. and Lee Vining) and two explosions (Kearsarge, $M_b = 5.6$; and Floydada, $M_b = 4$). The middle column contains the broadband response (amplitude in cm), the column on left contains the short-period response (Wood-Anderson) and on the right is the long-period response (Press-Ewing). The top three events have similar M_L 's.
3. Map locating events discussed in Figure 2 with respect to the recording stations PAS. Note the similarity in paths for Skull Mtn. and Kearsarge.
4. Observations from a small Yucca Flat explosion, Floydada ($M_L = 4.0$), recorded at TERRAscope stations and simulated Press-Ewing (long-period) and Wood-Anderson (short-period), after Woods *et al.* (1993).
5. Plot of M_L vs. M_0 for a population of explosions and earthquakes, after Woods *et al.* (1993).
6. Display of velocity vs. depth models for a southern California model (SC) and a basin-and-range model (PB).
7. Map of southwestern United States displaying the locations of a number of recent earthquakes and NTS explosions; also included is the TERRAscope array as existed in early 1993.
8. Comparison of broadband observations (Utah event) and corresponding synthetics (PB) as determined in obtaining the best fitting mechanism. The numbers indicate the peak amplitudes in cm. The numbers below the stations indicate the distance from that station to the event in kms.
9. Comparison of synthetics vs. observations for the Utah event where the time history has been adjusted such that the energy ratio between the synthetic (WASP/LP) in the *Pnl* window is equal to that observed as averaged over the 5 stations.
10. Waveform misfit errors as a function of dip and rake for one of southern California events (May 25, 1992, 12:22). a) The misfit error using normalization (expression (3) in the text). The misfit error is calculated using the true amplitude of the recorded waveforms (expression (4)). The global minima from the grid search are indicated by black dots.
11. The event location (star) and recorded waveforms (thickened traces) used in Figure 10. The synthetics above and below the data correspond to the solutions of Figure 10a and 10b respectively. Reference lines are arrivals of Love waves as determined from the tangential components.

12. Misfit errors of different portions of seismograms of 335 southern California events. True amplitude waveforms are used in the inversion. We chose $r_0 = 100$ km as reference distance. The solid lines are where the p values are determined from a least square fit.
13. Upper panel displays the SCEC catalog M_L vs. M_O determined by waveform inversion. These results can be compared against the relation determined by Thatcher and Hanks (1973). Lower panel contains the depths estimated from waveform inversion vs. the SCEC catalog.
14. Histograms of the depth distribution of earthquakes occurring in southern California as determined by TERRAScope. a) SCEC catalog depths; b) waveform inverted depths.
15. Comparison of predicted short-period synthetics vs. observations for the Utah event assuming the broadband time history.
16. Plot of accumulated energy for all three components (broadband) vs. distance for the three calibration events.
17. Comparison of data (small explosion) with synthetics (assumed to be double-couple). In this case the code found essentially a strike-slip solution. The depth of 5 km was determined by the best fitting solution. Note that there are many more scattered arrivals in the data that are not in the synthetics.
18. Plot of (M_E/M_B) vs. M_O for a small population of earthquakes and NTS explosions displaying good separation.
19. Plot of the short-period:long-period discriminant for a population of events, after Woods and Helmberger (1996).
20. Comparison of short-period energy curves of explosions and earthquakes (Skull MTN) at the various stations.
21. Upper panel displays a 2D cross-section from Imperial Valley (left) to Pasadena (right), distance is about 260 km. Lower panel displays the comparison of a relatively simple event (AN) compared to the more complex-looking event which occurred in the basin (IV). These are long-period comparisons with synthetics predicted from the above model.
22. Comparison of the broadband and Wood-Anderson short-period (WASP) vertical displacement data and cumulative energy curves for stations GSC and PFO for 3 Northridge aftershocks at different depths. In the displacement columns, numbers indicate epicentral distances. in the energy column, the short-period to broadband energy ratios are shown for each record. Note the degree of complexity as a function of source depth and station.

TRANSPORTABLE TIME DOMAIN DISCRIMINANTS

DON V. HELMBERGER, LUPEI ZHU, AND LARRY BURDICK

Seismological Laboratory 252-21

California Institute of Technology

Pasadena, CA 91125

Abstract

We have examined broadband waveforms from a large number of NTS explosions and earthquakes throughout the southwestern United States in order to characterize seismic sources. Explosions were found to be richer in coda energy than earthquakes. Most earthquakes show relatively little long-period ($T > 4$ sec) coda energy and tend to be richer in long-period and shear-wave energy than explosions. We have developed several seismic discriminants based on these observations and our modeling experience. One promising discriminant is the ratio of short-period vertical component, P-wavetrain energy, to long-period surface wave energy, averaged over three components. Explosions tend to have a higher ratio than do earthquakes, essentially an extension of $m_b:M_s$. Magnitude threshold for this discriminant is about 3.5. Another useful discriminant is based on the total broadband energy to moment ratio where explosions are distinguished by their stronger energy levels relative to their long-period amplitudes. This approach requires Green's functions, a source estimator program, and processes all events as earthquakes. For this method to be effective requires the calibration of the region using relatively large earthquakes, $M > 5$, but does not require calibrations of explosions.

1. Introduction

A number of broadband arrays have been introduced in recent years. One such array, TERRAScope, is presently being installed in southern California, see Figure 1. These stations are a part of the global IRIS (International Research Institution for Seismology) network. Presumably the IRIS network, in conjunction with short-period arrays, will provide some of the essential data necessary for worldwide monitoring of seismic activity. Unfortunately, station spacing in remote areas is rather sparse. Thus, we may have to rely on a single station to characterize events and to distinguish an explosion from an earthquake. This task will be difficult, but may be possible in regions that have an abundance of earthquakes that can be used to calibrate regional paths. We envision an environment not unlike that of western United States and thus we can use the

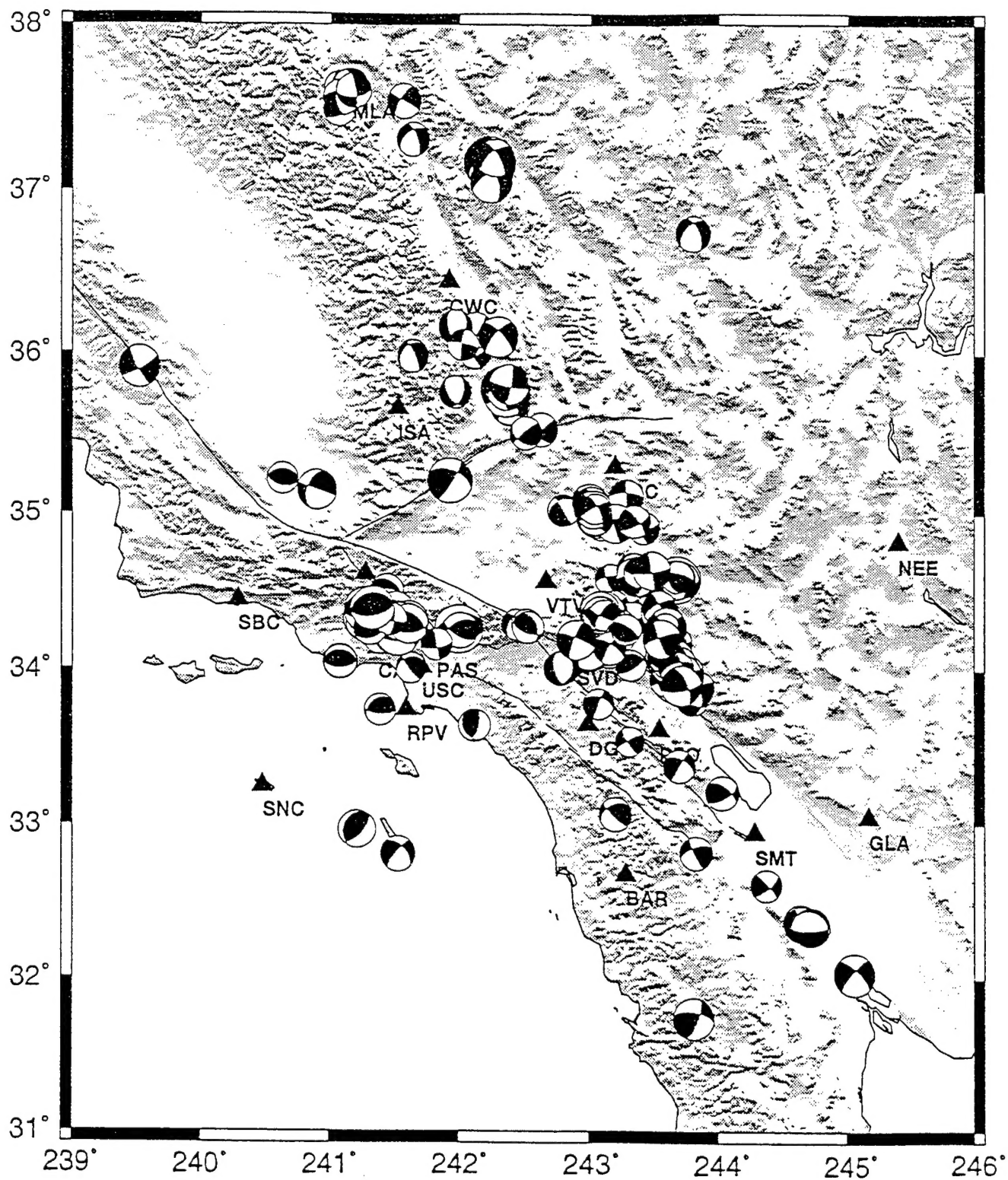


Figure 1

population of NTS events and the natural seismicity to construct and test such a methodology. Before discussing regional calibration and the development of energy discrimination techniques, we will first briefly review the observational differences between explosions and earthquakes.

Most of the useful regional discriminants for populations of explosions and earthquakes in this region have been discussed by Taylor *et al.* (1989). Their results suggest that $m_b \cdot M_s$ works very well for well-calibrated paths but they had difficulty in determining M_s for explosions smaller than about $m_b=4$. In contrast, they report M_s for earthquakes with m_b 's as small as 2.5. The characteristics of events as described above are quite compatible with TERRAscope observations, as displayed in Figure 2, where seismograms of the Kearsarge explosion is compared with the Skull Mountain and the Lee Vining earthquake. The locations of these events and the recording station are shown in Figure 3. The earthquakes were chosen to be ones that have source to receiver paths similar to that of NTS explosions so that propagation effects are minimized. The middle column displays the broadband records. The waveforms on the left are convolved with a short-period instrument, and the waveforms on the right are convolved with a long-period instrument. Peak amplitudes are printed to the right of each trace. Comparing the ratio of peak short to long-period amplitudes (column 5, Table 1), it is apparent that the explosions are richer in high frequency energy relative to the earthquakes.

Below, each seismic trace is its energy integral. The short to long-period energy ratios show similar trends. For the earthquakes there are two large step increases in the energy; the first is the P-wave train and the second is at the onset of the S-wave train. Although the explosions show the same behavior, the second step is not as pronounced, as explosions tend to generate relatively small amounts of shear wave energy. If the short-period energy is only integrated over the P-wave train window (approximately the first 40 sec. of the wave train), the short to long-energy ratio should show even greater separation between the two source types as discussed later. Simulations of the broadband data appropriate for various instruments are included since this type of data is normally used in defining m_b and M_L (WASP), and M_s (LP). Note that because the paths are nearly identical, this difference must be caused either by the source excitation and/or epicenter depth. Thus, it appears that $m_b \cdot M_s$ can be extended to small events if the Rayleigh waves can be detected.

In Figure 4, we display more of TERRAscope data for the small NTS explosion Floydada where the Rayleigh waves are quite apparent even at long-periods. Note that the surface wave amplitudes indicate that these signals would not be discernible on the actual analog instruments. M_L for this event is 4.0 and its log moment is 14.20, Woods *et*

Skull Mtn, Lee Vining, Kearsarge and Floydada at PAS, Vert. comp.

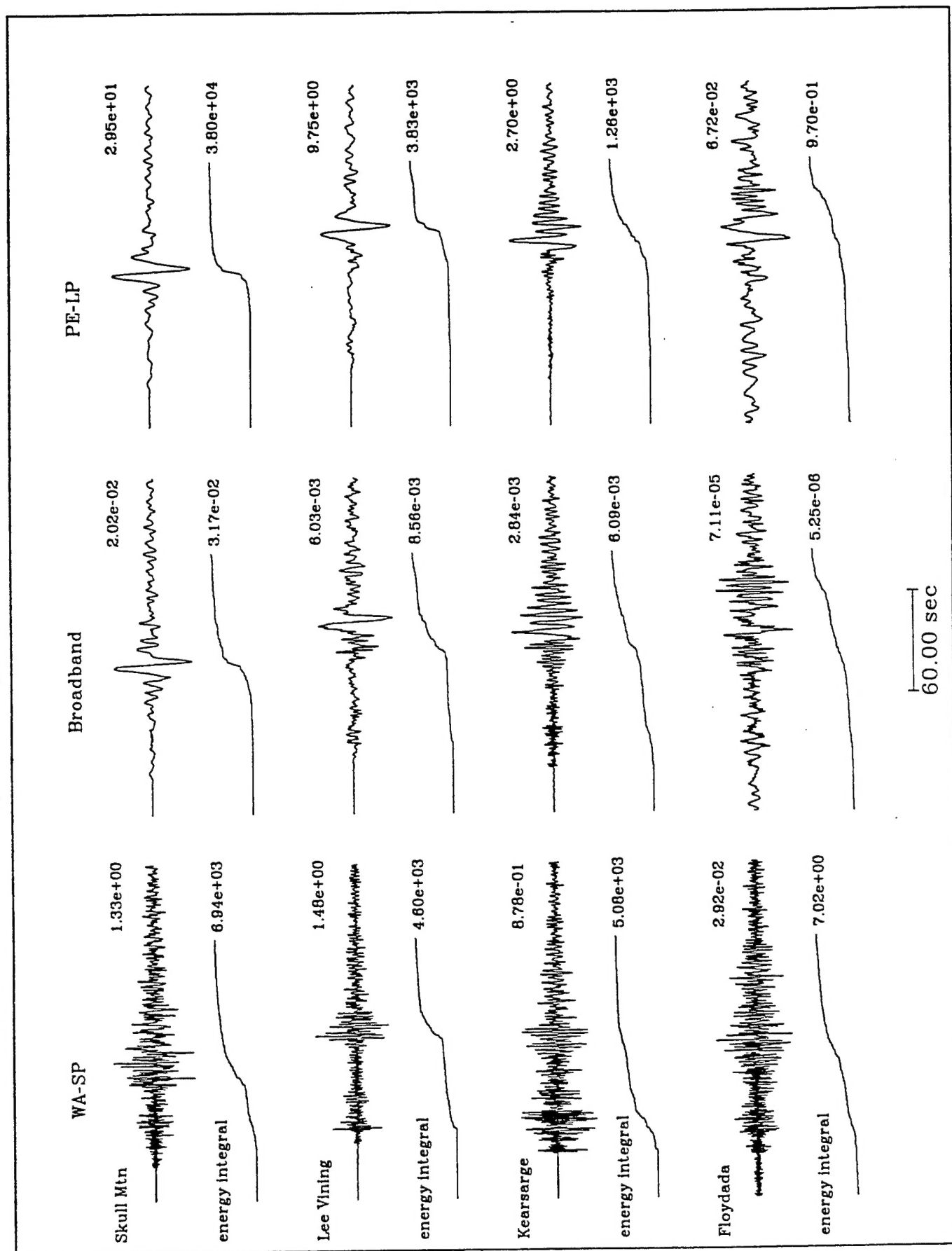


Figure 2

Study Area

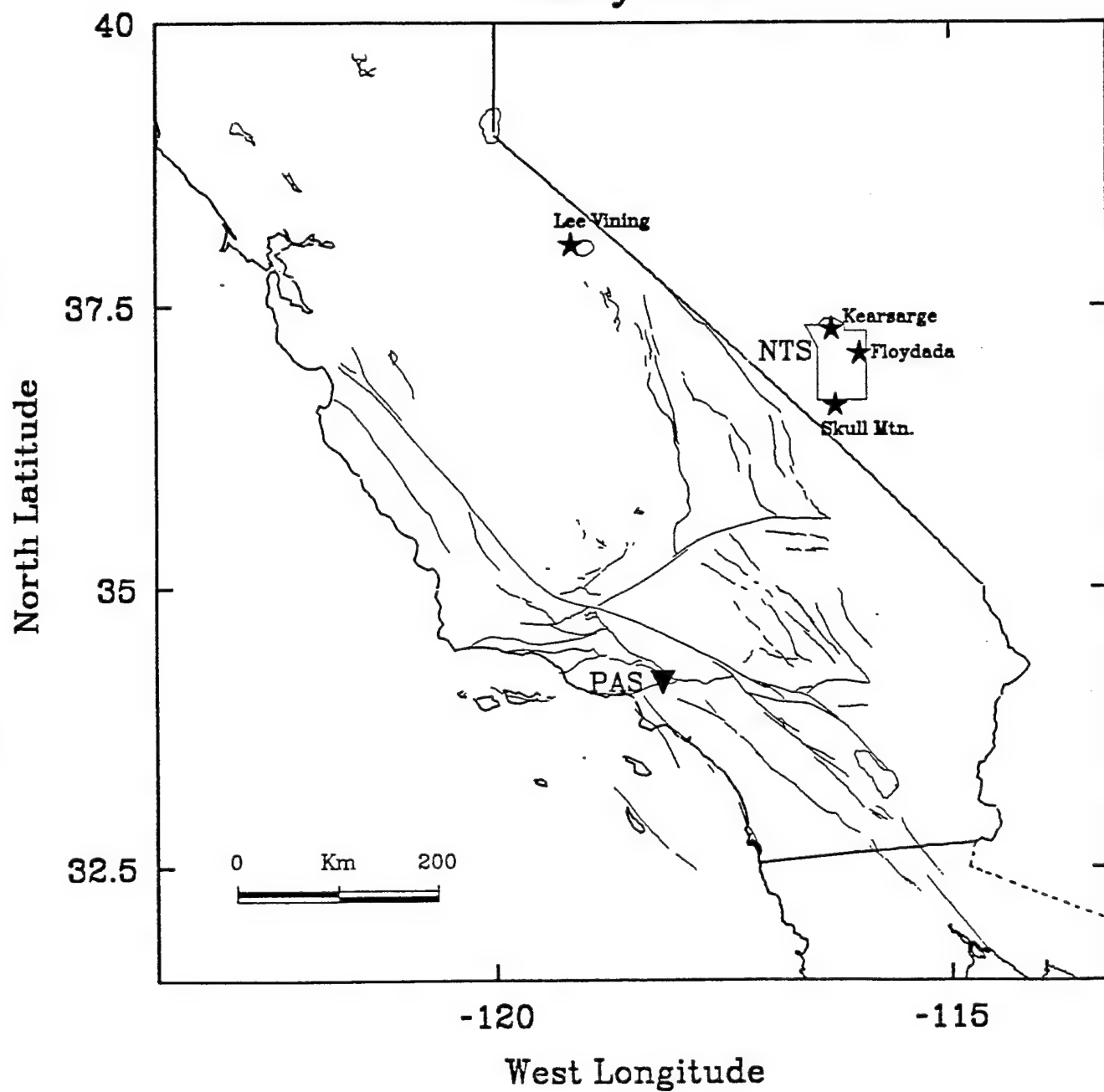


Figure 3

al. (1993). Assuming it is a shallow explosion above the water table, the yield can be inferred to be less than 10 kt from the moment-yield scaling relationships determined for NTS by Woods and Harkrider (1994). Were it detonated in hard rock below the water table it would correspond to a two kiloton explosion. We estimate that were this event 2.5 times lower in yield, it would still be possible to obtain its moment, yielding a magnitude threshold of about 3.5. These observations are quite typical of small NTS events where only the fundamental Rayleigh wave Airy phase is detectable and reasonably predictable across the array.

Thus, it appears that regional seismograms from explosions are indeed higher frequency than earthquakes with comparable Rayleigh wave excitation. This feature is explored by Patton and Walter (1993), in a study of well-calibrated $m_b:M_s$ and the $m_b:M_0$ discriminants. Their results produced a clear separation as does the $M_L:M_0$ discriminant proposed by Woods *et al.* (1993). The latter results are displayed in Figure 5. Note there is a significant separation of earthquakes and explosions with no real overlap over all scales. However, many of the M_0 's for these explosions were determined by assuming shallow isotropic excitation (Woods *et al.*, 1993), and thus while this approach demonstrates that the high-frequency vs. low-frequency source characterizations remain valid to small magnitudes, it may have limited usefulness as a direct discriminant.

Another difficulty with the $M_L:M_0$ discriminant is in the development of a physical basis. While the M_L measure is easily simulated for earthquakes it proves problematical for explosions. For example, in examining Figure 4, we find that the peak short-period amplitude usually occurs on the tangential component. This is difficult to explain with the conventional symmetric RDP (Reduced Displacement Potential) formalism and require some type of mode conversion. Presumably, the large amount of local Rayleigh wave energy released by the source into the slow-velocity source region gets scattered into the crustal wave guide (e.g., Stead and Helmberger, 1988). We find the broadband (BB) records from earthquakes occurring in the normal seismogenic depths of 4 to 15 kms to be relatively simple as discussed in the next section. Thus, we will explore the possibility of using the ratio of accumulated energy to surface wave magnitude or M_0 as a discriminant.

To pursue this approach we will assume all events are earthquakes with respect to estimating source parameters. Explosions are then distinguished by their excess short-period energy. However, to obtain meaningful estimates of source parameters from regional waveforms does require a crustal model and useful Green's functions. These can be obtained by modeling moderate sized earthquakes.

Table 1: Discrimination Parameters for Figure 2 Events

Event	M_L	$\log(M_0)$	$\log(M_0) - M_L$	SP-LP Amp. Ratio	SP-LP Energy Ratio	SP(P-wave)-LP Energy Ratio
Skull Mtn.	5.6	17.4	11.8	0.045	0.18	0.045
Lee Vining	5.0	16.7	11.7	0.150	1.20	0.380
Kearsarge	5.5	15.6	10.1	0.33	4.03	1.84
Floydada	4.0	14.2	10.2	0.43	7.24	2.78

Floydada (Yucca Flats), $M_L=4.0$

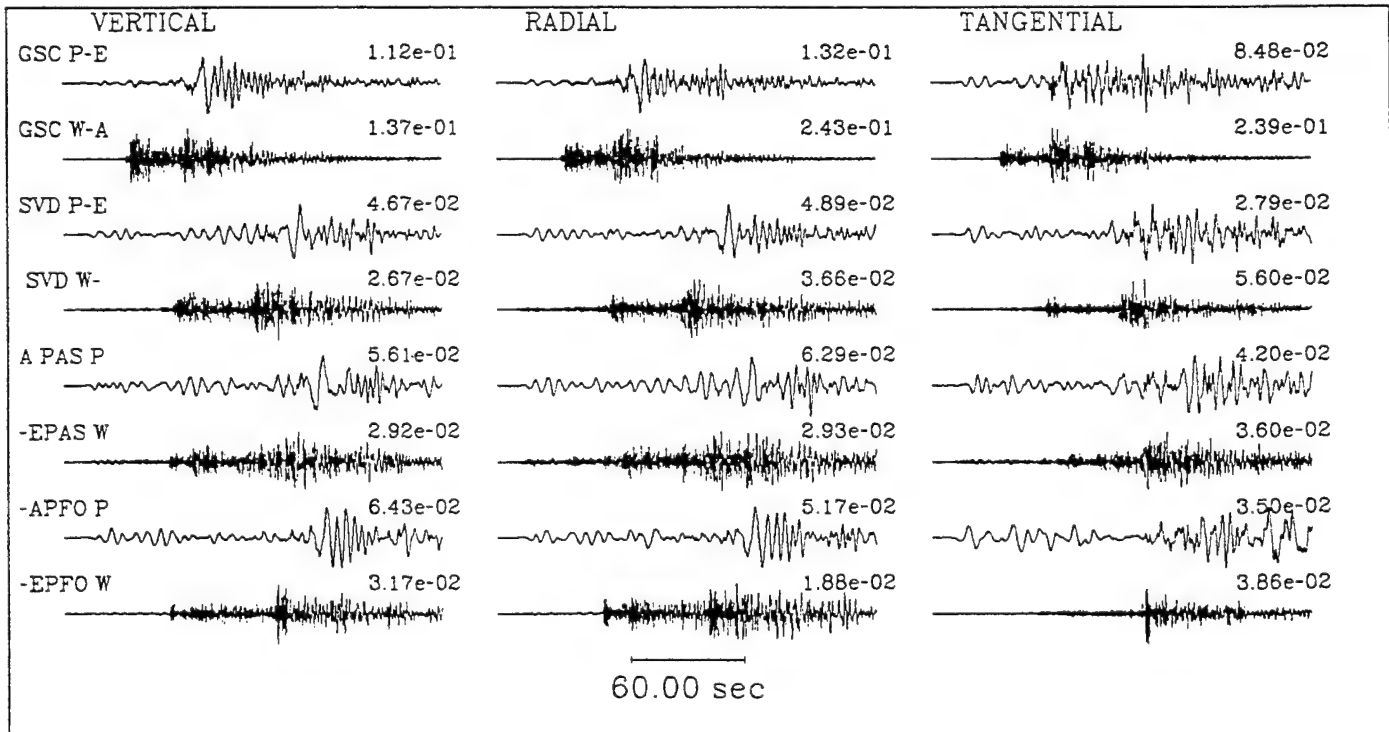


Figure 4

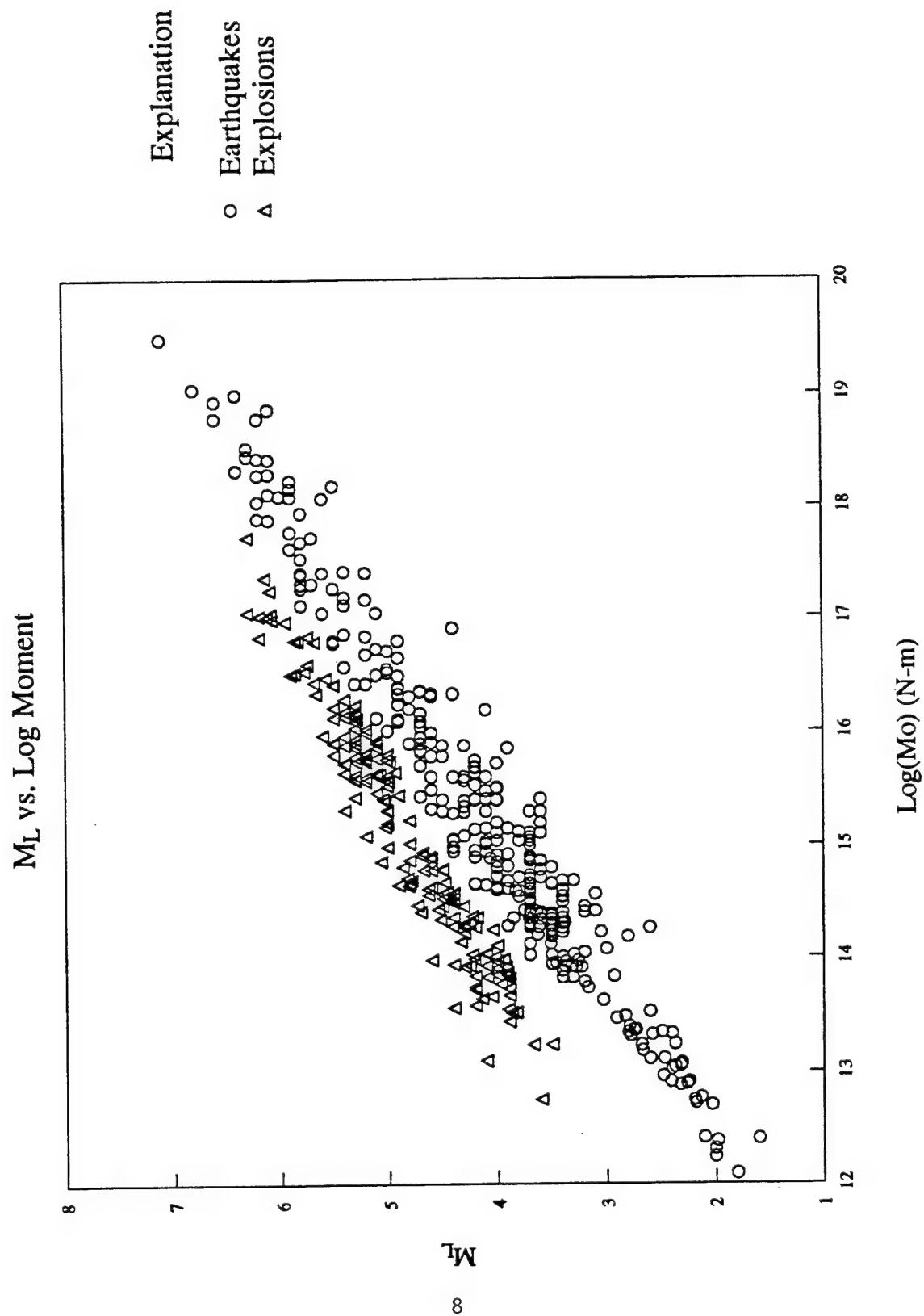


Figure 5

2. Estimation of Earthquake Parameters

Essentially, three new methods have been developed to take advantage of the new instrumentation: the CMT (Centroid Moment Tensor) solution at long-periods, Patton (1980), Thio and Kanamori (1995), and others, (Ritsema and Lay, 1993), inversion of long-period body waveforms (Dreger and Helmberger, 1993), Fan and Wallace (1991) and others, and a broadband cut and paste (CAP) method by Zhao and Helmberger (1994).

For events larger than $M_w > 5$, it is possible to invert surface wave records for periods greater than 50 seconds assuming the PREM model (Dziewonski and Anderson, 1981) by employing a CMT procedure. At shorter periods the surface waves show regional variation, and corresponding regionalized models are required (see for example, Patton and Zandt, 1991; Thio and Kanamori, 1992).

The second method uses the relative strengths of the observed body waves compared with synthetics to determine mechanisms, moment, and depth. Often, only one station is sufficient to fix the source parameters, since S (SV and SH) and sS (SV and SH) are strongly dependent upon source orientation. Cycling through source depths the proper timing between P and pP, S and sS can be established, etc. allows accurate depth estimates. This approach works best at periods greater than a few seconds and therefore we usually work with long-period bandpassed records. The Southern California model (SC), Dreger and Helmberger (1991), displayed in Figure 6 works well in terms of producing synthetics that match data throughout the entire region, as reported by Dreger and Helmberger (1993).

The third approach uses a direct grid search for the fault parameters (strike (θ), dip (δ), rake (λ)). This method matches complete broadband observed seismograms against synthetics over discrete phases so that timing shifts between particular wave groups are allowed. That is, in matching a synthetic seismogram to the observed record, we may allow the Rayleigh wave to be shifted relative to the P_{nl} wavetrain. This allows a better correlation, thus the name cut-and-paste method (CAP). This feature desensitizes the effect of the crustal model used in generating the synthetics and allows stable estimates of the source parameters with imperfect Green's functions. We demonstrate this conjecture by generating fault parameters for a number of regional events using two strongly contrasting crustal models, the SC model and a basin and range model (PB) by Priestley and Brune (1978), displayed in Figure 6. The source parameter determinations are given in Table 1 for three large events in the region: the Utah event, the Little Skull Mountain event, and the Arizona event. Paths connecting these events to the

TERRAscope stations provide a good sample of the propagational features of the region, see Figure 7.

A comparison of the waveform fits assuming the PB model is displayed in Figures 8 and 9. The numbers above each trace indicates the peak amplitude and the moment estimate comes from a least square fit where the individual amplitude comparison indicates the relative contribution of that trace to the average moment. The relative shifts of the various phases is discussed in Zhao and Helmberger (1994).

3. Source Estimation Using True Amplitude Waveforms

Let $u(t)$ be the observed displacement. The corresponding synthetic displacement $s(t)$ for a double-couple source can be expressed as:

$$s(t) = M_0 \sum A_i (\phi - \theta, \delta, \lambda) G_i(t), \quad (1)$$

here, $i=1,2,3$ corresponds to three fundamental faults, i.e., vertical strike-slip, vertical dip-slip, and 45° dip-slip. G_i 's are the Green's functions, A_i 's are the radiation coefficients, and ϕ is the station azimuth. M_0 is scalar moment; θ , δ , and λ are strike, dip, and rake of the source that we want to determine from $u(t)$. They can be estimated by solving the equation

$$u(t) = s(t). \quad (2)$$

Since there are only limited unknown parameters and all of them are limited to a range of values ($0 \leq \theta \leq 2\pi$, $0 \leq \delta \leq \pi/2$, $0 \leq \lambda \leq 2\pi$), it is convenient to solve the above non-linear equation by grid search method. We define an object function to measure the misfit error between u and s and search through the parameter space to find the global minimum of the object function.

In Zhao and Helmberger (1994), the misfit error is defined as the norm ($L1$ or $L2$) of the difference between u and s normalized by the norms of both u and s :

$$e = \frac{\|u - s\|}{\|u\| + \|s\|}, \quad (3)$$

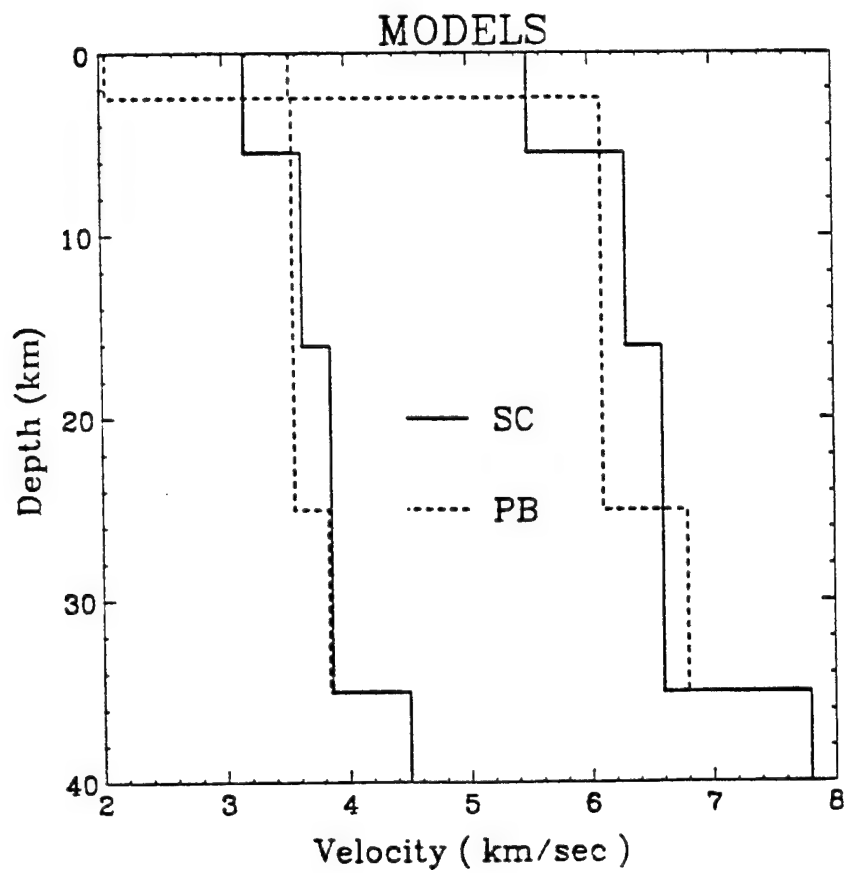


Figure 6

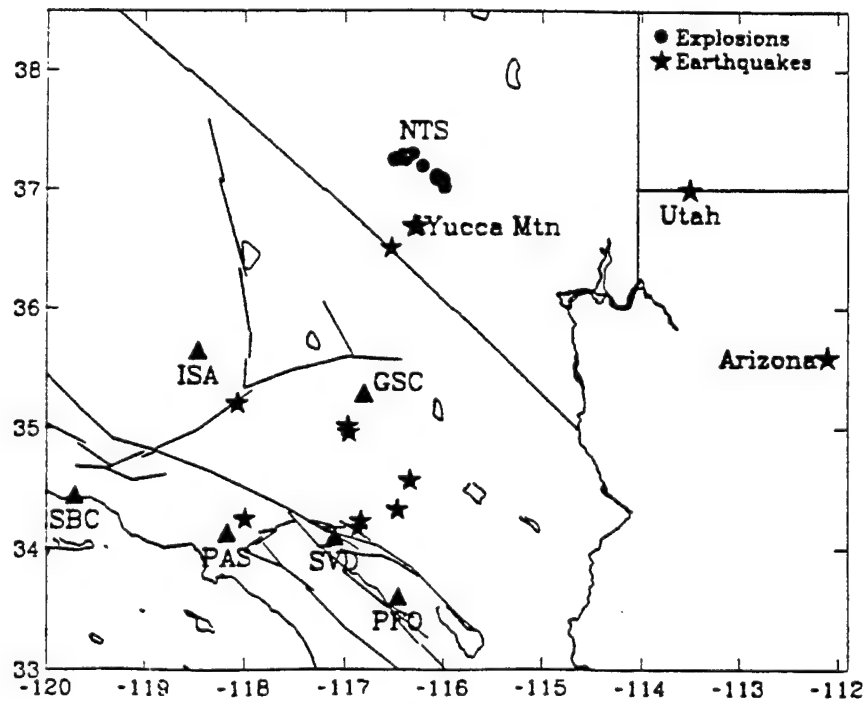


Figure 7

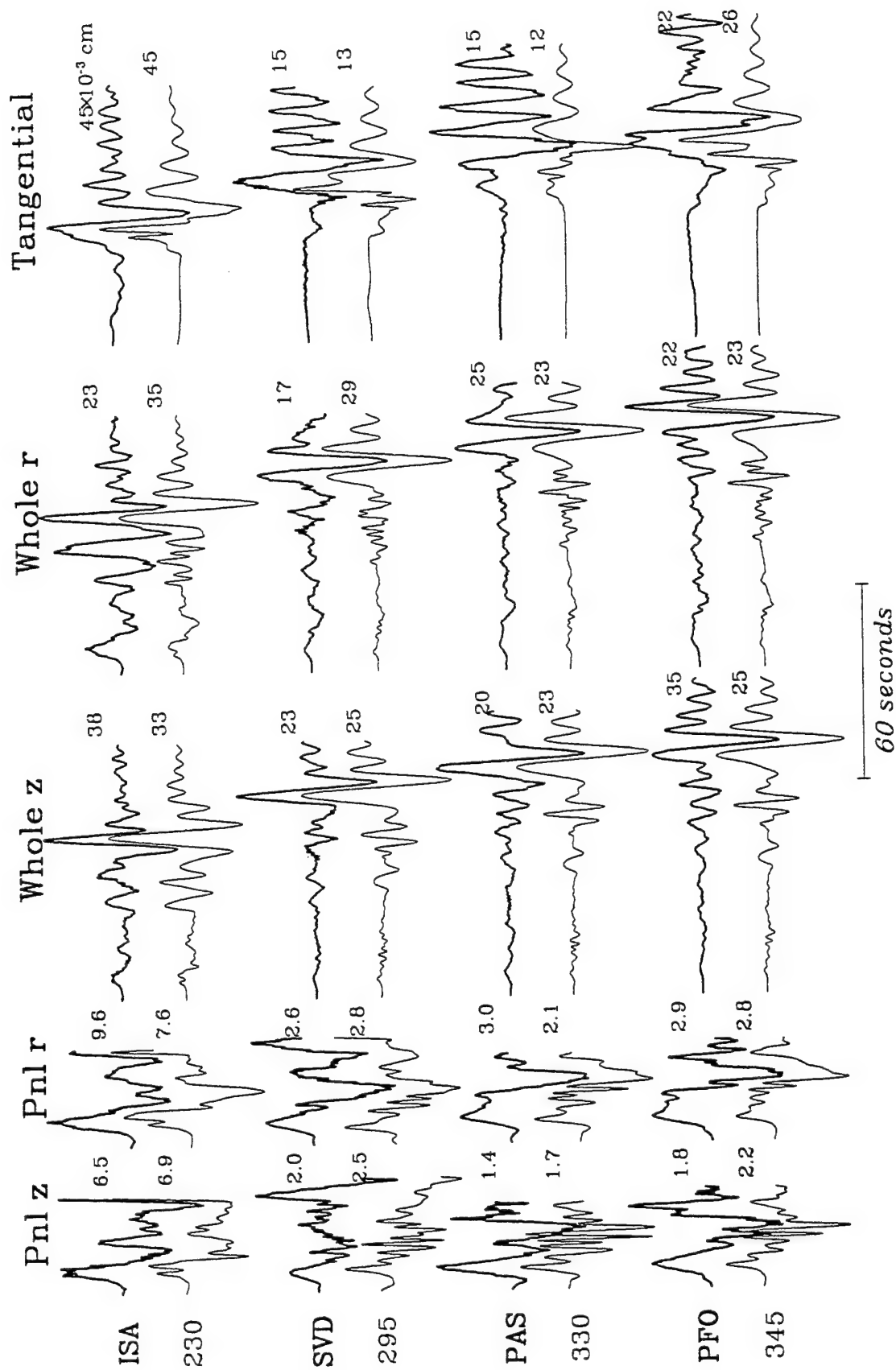


Figure 8

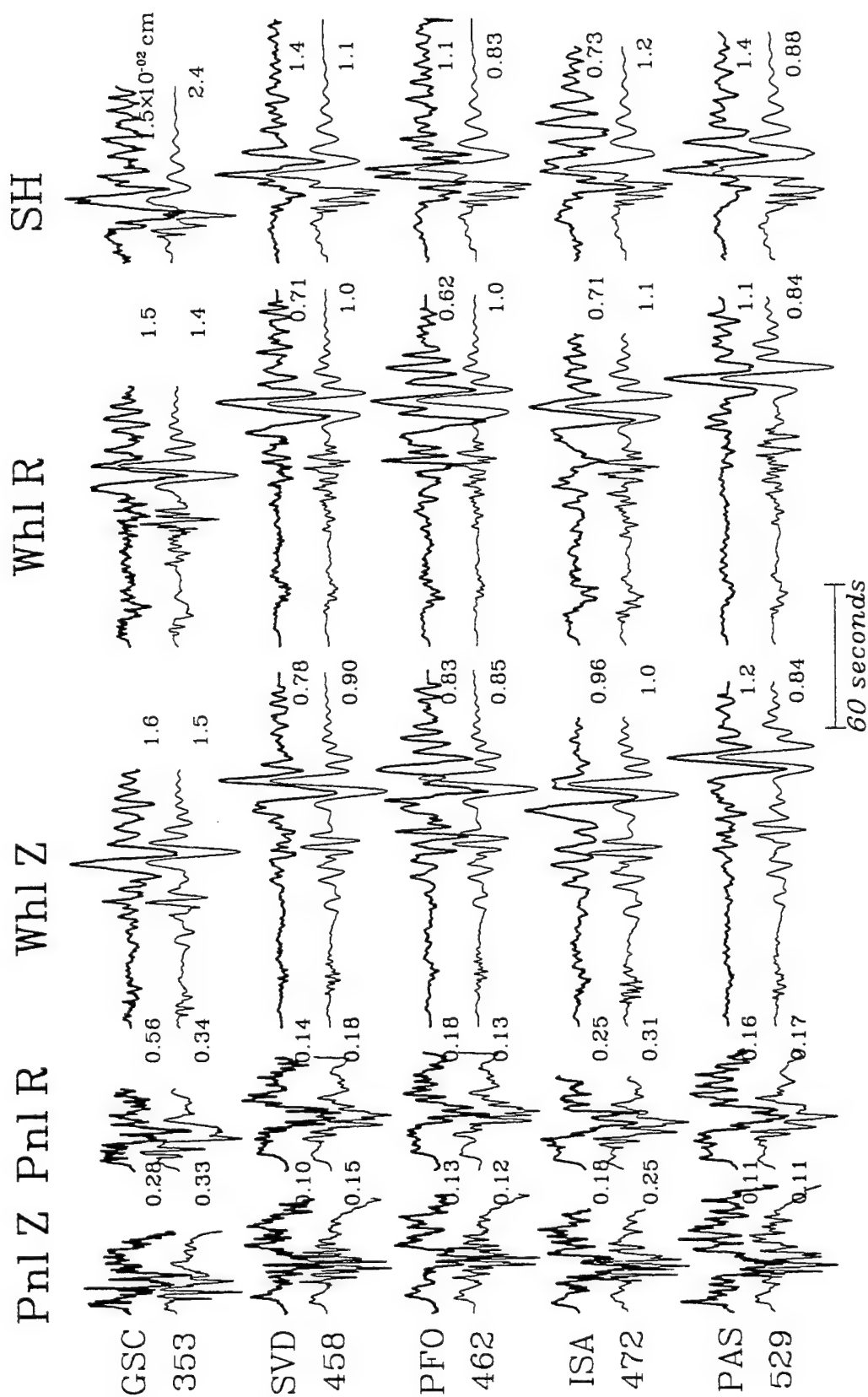


Figure 9

Because *Pnl* usually has smaller amplitude than surface waves, this normalization helps to weight *Pnl* and surface waves equally. It also prevents the inversion from being complete dominated by the strongest station, which is usually the nearest station, if several stations at different distance ranges are used. However, the amplitude information is lost during the normalization. Some of this information, such as amplitude ratios of *Pnl* to-surface waves and *SV*-to-*SH*, provide important constraints on the source orientation and depth. A more severe problem with this normalization is that it introduces singularities in the source parameter space at those points where source orientation generates nodal synthetics (where the norm of the synthetics vanishes). In the case when the data includes nodal records, the grid search will miss the true minimum.

As an example, Figure 10 shows the misfit error as defined by (3) as a function of dip and rake (the location of the event and the waveforms are displayed in Figure 11). The global minimum is very obscure. The error surface is distorted by some peaks and ridges which are associated with singularities introduced by the normalization. Figure 10b is the misfit error using true amplitudes without normalization:

$$e = \| u - s \| . \quad (4)$$

It has a well defined minimum at $\delta = 80^\circ$, $\lambda = -15^\circ$. Note that the *P-SV* waves at station PFO, GSC, and ISA are close to nodal (Figure 2), which are well matched by the solution. But the solution in Figure 10a is offset by 15° in rake and the corresponding synthetics have larger *P-SV* amplitudes compared with the data (Figure 11).

This particular example of waveform modeling exposes the difficulties encountered at nodes. Since the *P-SV* motions are near nodal to the north, the radial and vertical components are easily contaminated by *SH* motions (see reference lines in Figure 11). The "cut and paste" aspect of the search procedure moves the synthetic Rayleigh wave forward attempting to capture some of this energy to constrain mechanism. The modified method tends to suppress such spurious attempt. However, its M_0 estimation could be somewhat low since scattered energy is less well sampled, as suggested in this comparison.

Using true-amplitude waveforms for source inversion usually leads to the problem of the closest station dominating the inversion when stations are distributed over a large distance range. Figure 12 shows misfit errors as a function of distance. These misfit errors were obtained through a global search applying expression (4) to 335 southern Californian regional events of $M_L \geq 3.5$.

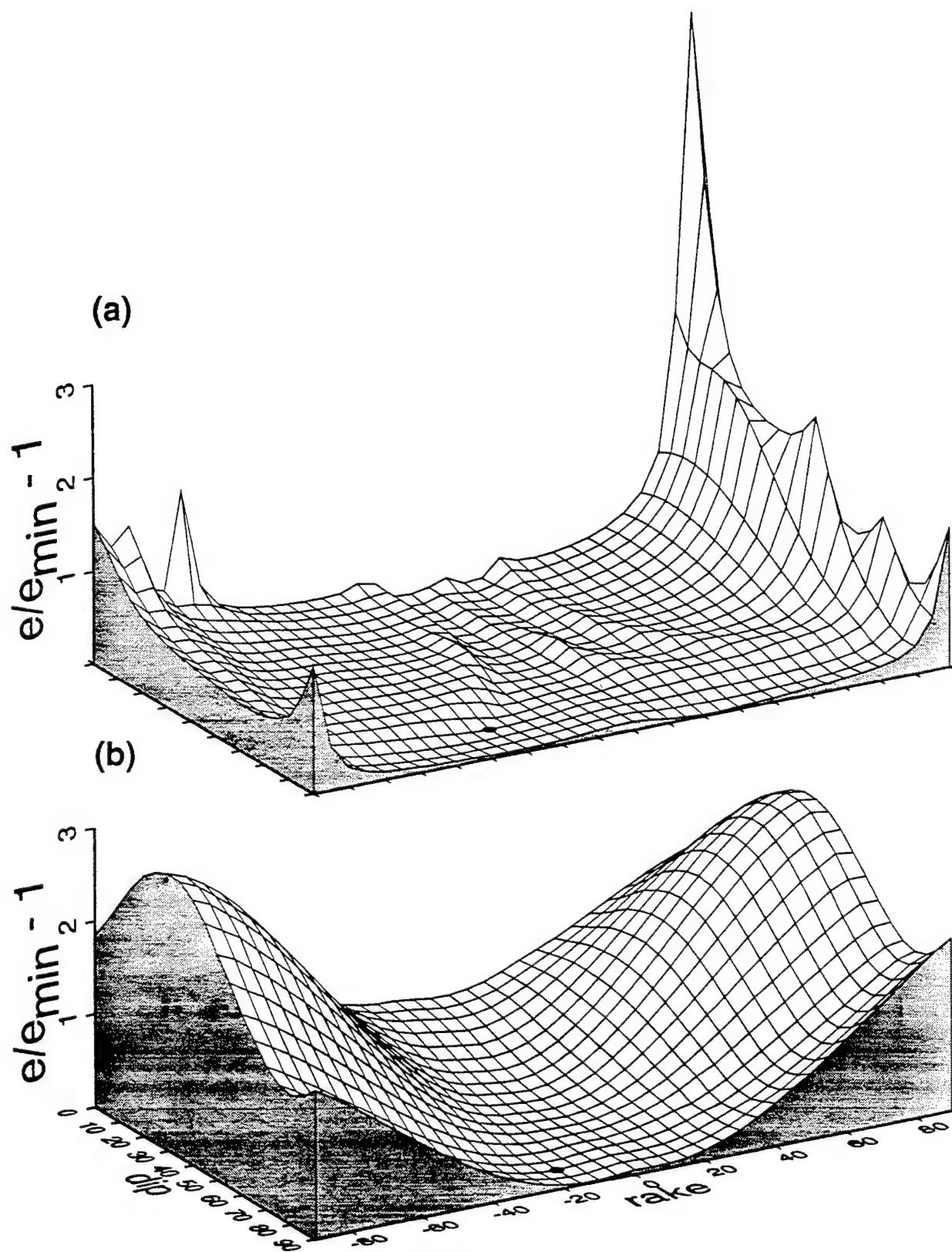
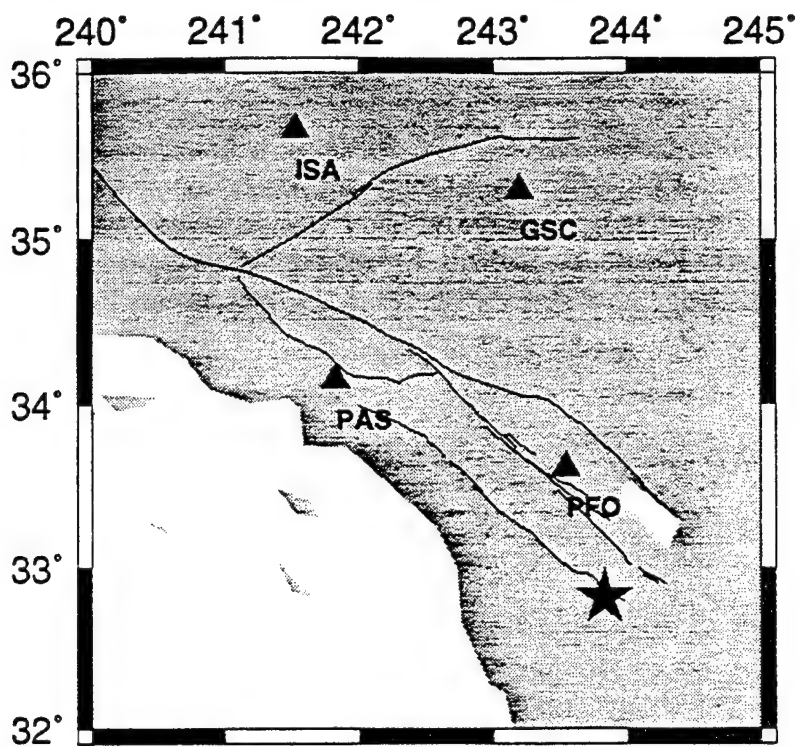


Figure 10



(a) 245/75/-30 Mw 4.0



(b) 250/80/-15 Mw 3.8

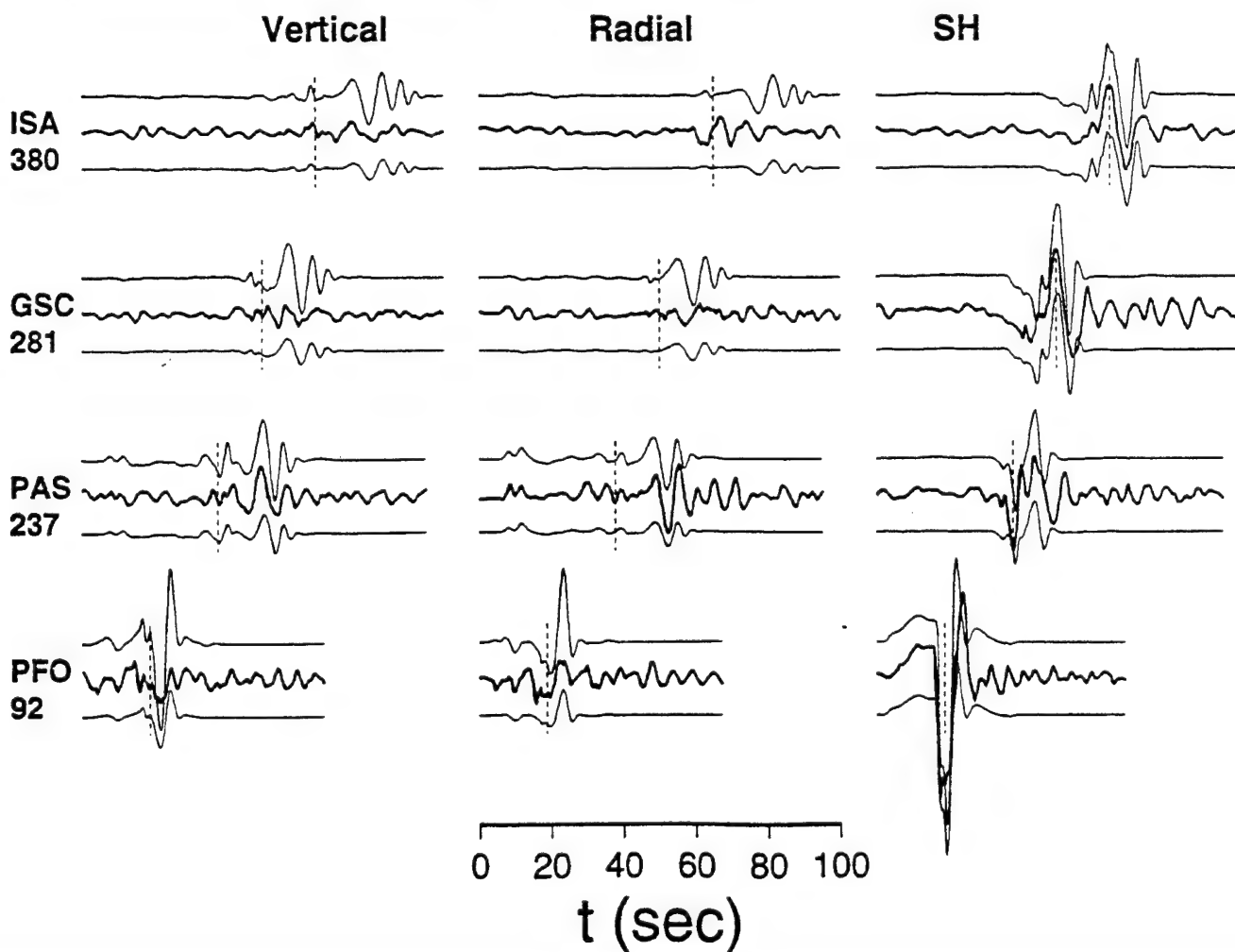


Figure 11

The misfits of surface waves have larger scatter than body waves, which are expected because surface waves are more easily affected by shallow heterogeneity. It has been shown that *Pnl* at range of 300 km to 1000 km is quite stable (Helmberger and Engen, 1980) and easily inverted for source mechanisms (Wallace and Helmberger, 1982). At closer range, the details of the moho transition plays a more important role as well as the PL waves trapped in the shallow crust (Song and Helmberger, 1996). Since both of these features show strong local variation, we should expect the large scatter displayed in Figure 12 at closer distances. However, because the *Pnl*'s at nearest stations play an essential role in early warning (Scrivner and Helmberger, 1996), the local structure should probably be added to each station. This approach will be pursued in future efforts.

Despite the scatter of data in Figure 12, the misfit errors show a rapid decay with distance. Since radiation patterns have been taken out, this decay is related to the amplitude decay due to geometrical spreading and attenuation. To compensate for this decay, we introduce a distance range scaling factor and define the misfit error for a record at a distance r as

$$e = \left\| \left(\frac{r}{r_0} \right)^p \cdot \| u - s \| \right\|, \quad (5)$$

here p is a scaling factor to give the record at r the same weight as that at reference distance r_0 . If we assume a spherical geometrical spreading for body waves and cylindrical geometrical spreading for surface waves, an appropriate choice of p would be $p=1$ for body waves, and $p=0.5$ for surface waves. For southern California, the p -values determined from Figure 12 are 1.13 for *Pnl*, 0.55 for Love waves, and 0.74 for Rayleigh waves. The scatter in the figure is large especially at the smaller distances, suggesting considerable variation in local structure and the need for regionalization. Nevertheless, it appears that the p -values derived from geometrical spreading are reasonably good for the period range (5 to 100 sec) used in waveform inversion.

We have applied the technique to all available regional events of $M_L \geq 3.5$ recorded by TERRAscope back to 1990. A total of 335 focal mechanism solutions are obtained. Although a large number of them are aftershocks of the 1992 Landers and 1994 Northridge earthquakes, the data set still gives a good sampling of active source regions in southern California (Figure 1). Figure 13 is the comparison of inverted focal depths and M_0 with the depths and M_L determined by the southern California short-period network (from Southern California Earthquake Center (SCEC) Catalog). M_0 vs. M_L

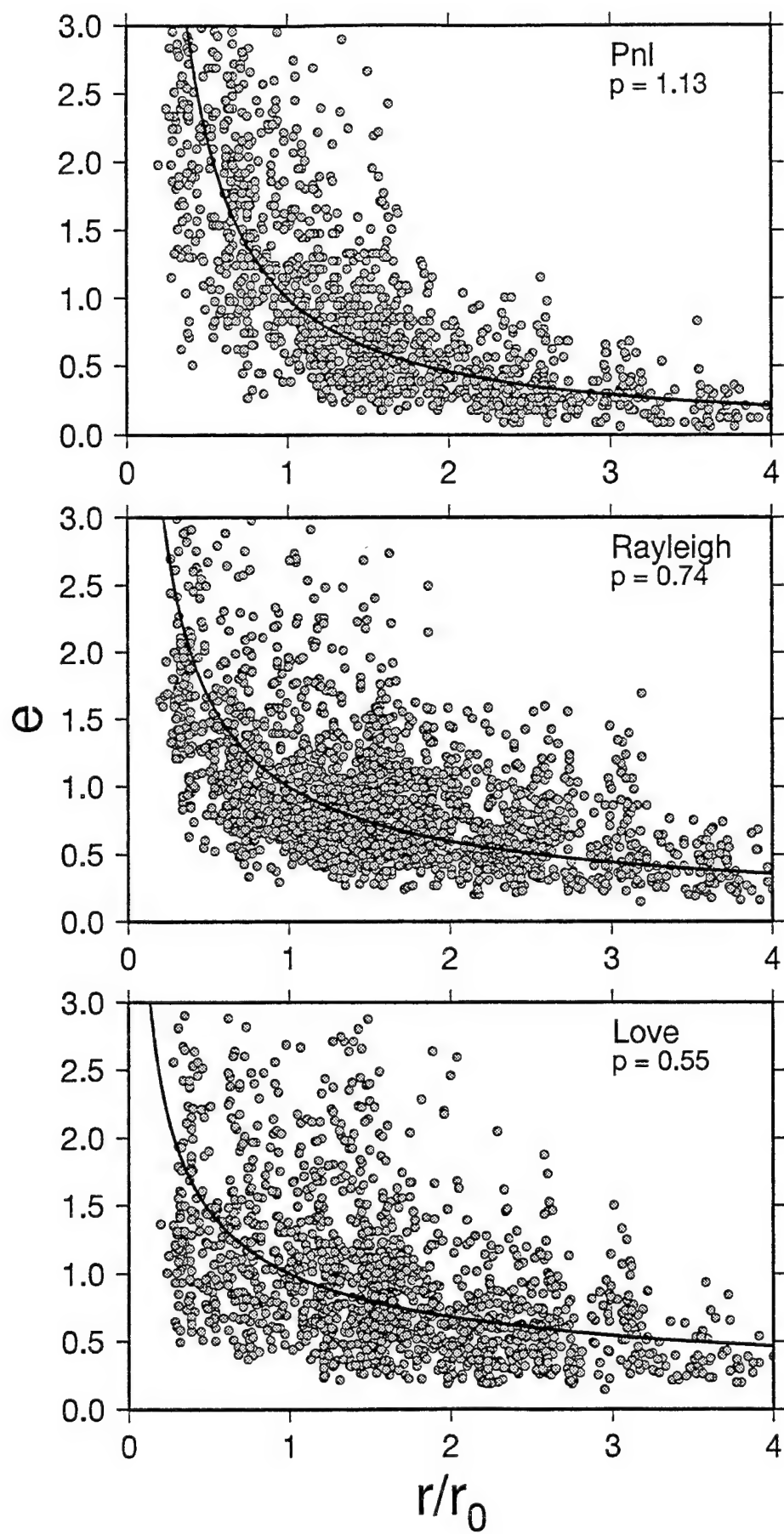


Figure 12
18

essentially follows the relation found by Thatcher and Hanks (1973). But the waveform inverted depths are generally deeper than the catalog depths.

4. Focal Depth Distribution and the Seismogenic Zone in Southern California

Figure 14 shows the histograms of SCEC catalog depths and waveform inversion depths for the 335 events in this study. The catalog depths are determined from arrival times on the southern California short-period network. Large uncertainty exists for these routinely determined depths, mostly due to the severe trade-off between depth and origin time. The most accurate information on depth distribution of seismicity is usually obtained from aftershock sequences during which temporary recorders are deployed directly above the rupture. However, the interpretation of aftershocks can be complicated because the mainshock greatly changes the local stress field. Preshocks and background events probably provide a more accurate picture of the evolving stress field. Since our waveform inversion technique conserves the amplitude information among various crustal phases, source depths should be better constrained, even for small magnitude earthquakes.

The depth distribution obtained from waveforms inversion shows a strong peak at about 12~km with few events occurring above 5~km and below 20~km. This seems quite compatible with the expected seismogenic zone for an tectonic active region as southern California. It is generally thought that the lower boundary of seismogenic zone is due to a transition from brittle to ductile behavior in continental crust (Meissner and Strehlau, 1982; Sibson, 1984; Doser and Kanamori, 1986). The top of seismogenic zone is controlled by a transition from stable sliding to stick slip, which can be attributed to the presence of unconsolidated fault gouge (Marone and Scholz, 1988). For a region overlain by sedimentary structures of unconsolidated material and with well-developed faults, they predict a minimum source depth of 3-5~km, which agrees well with our results.

5. Estimation of Seismic Energy and Discriminants

Because the misfit errors defined in Zhao and Helmberger (1994) and others (Wallace and Helmberger, 1982; Fan *et al.*, 1994) are normalized by the data and synthetics, the amplitude information in the data has not been fully utilized to constrain the source orientation and depth. Thus, we can strengthen the CAP technique by removing this normalization and allowing better use of amplitude information. As multiple stations at different distance ranges are often used in source inversion, we will also investigate the amplitude decay with distance range and correct it by introducing a distance scaling factor.

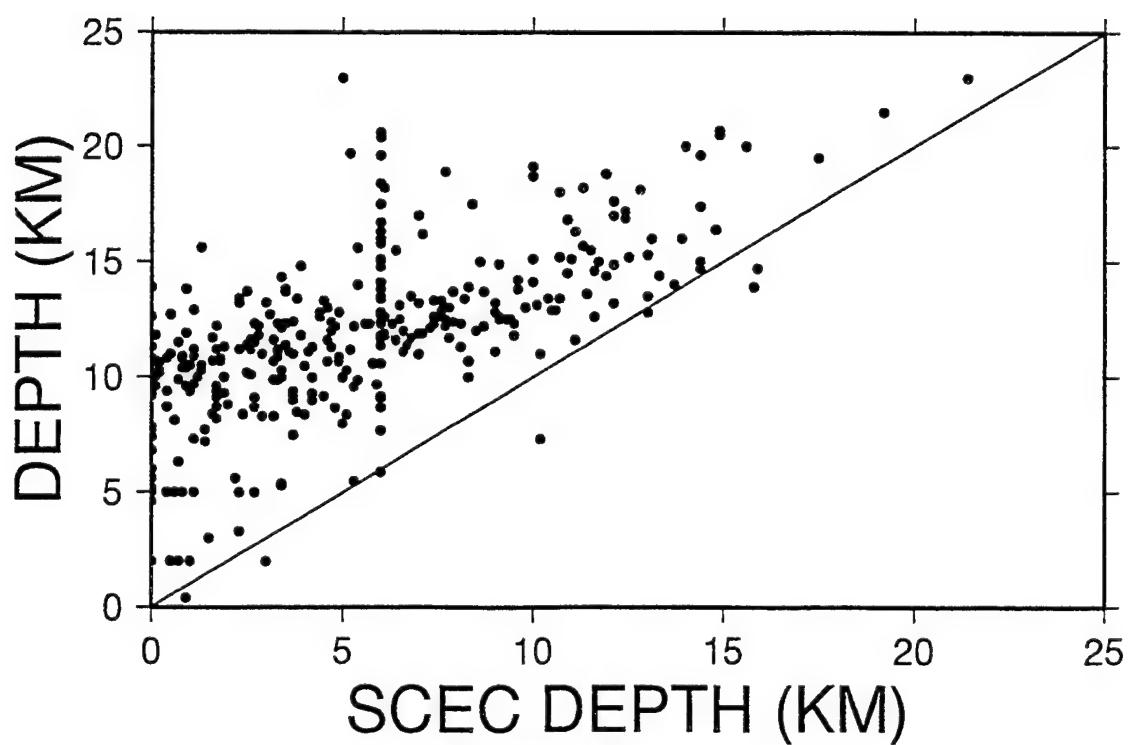
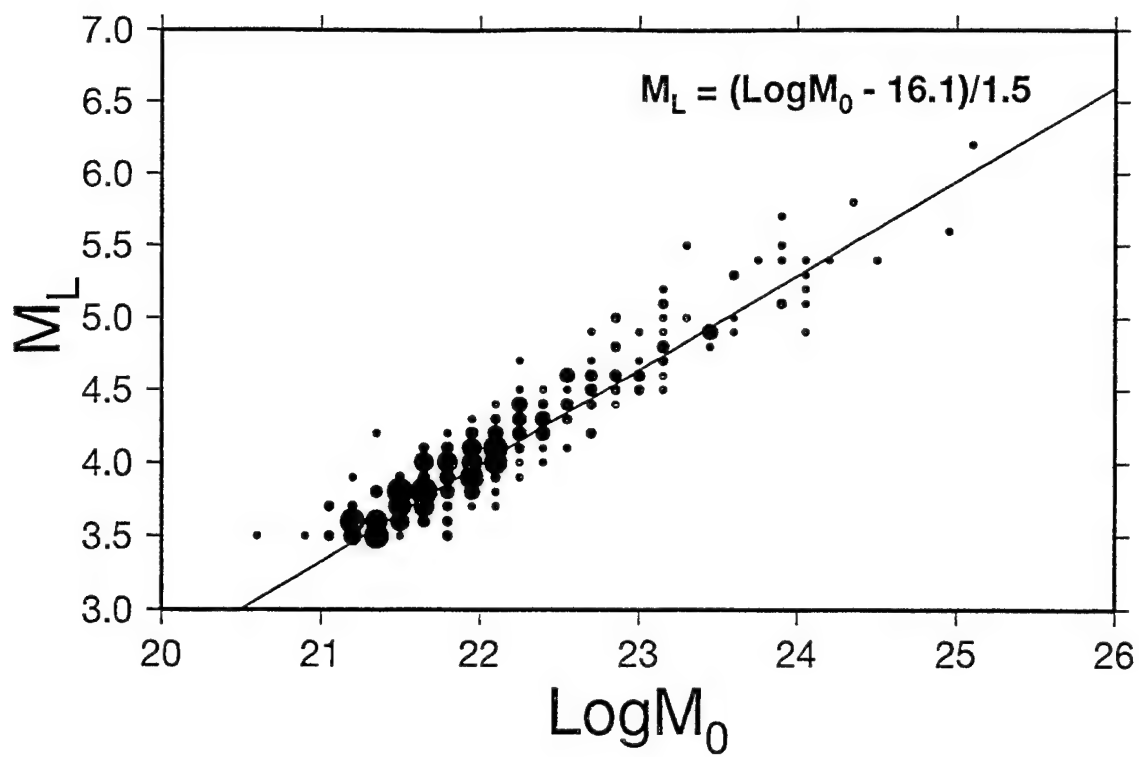


Figure 13

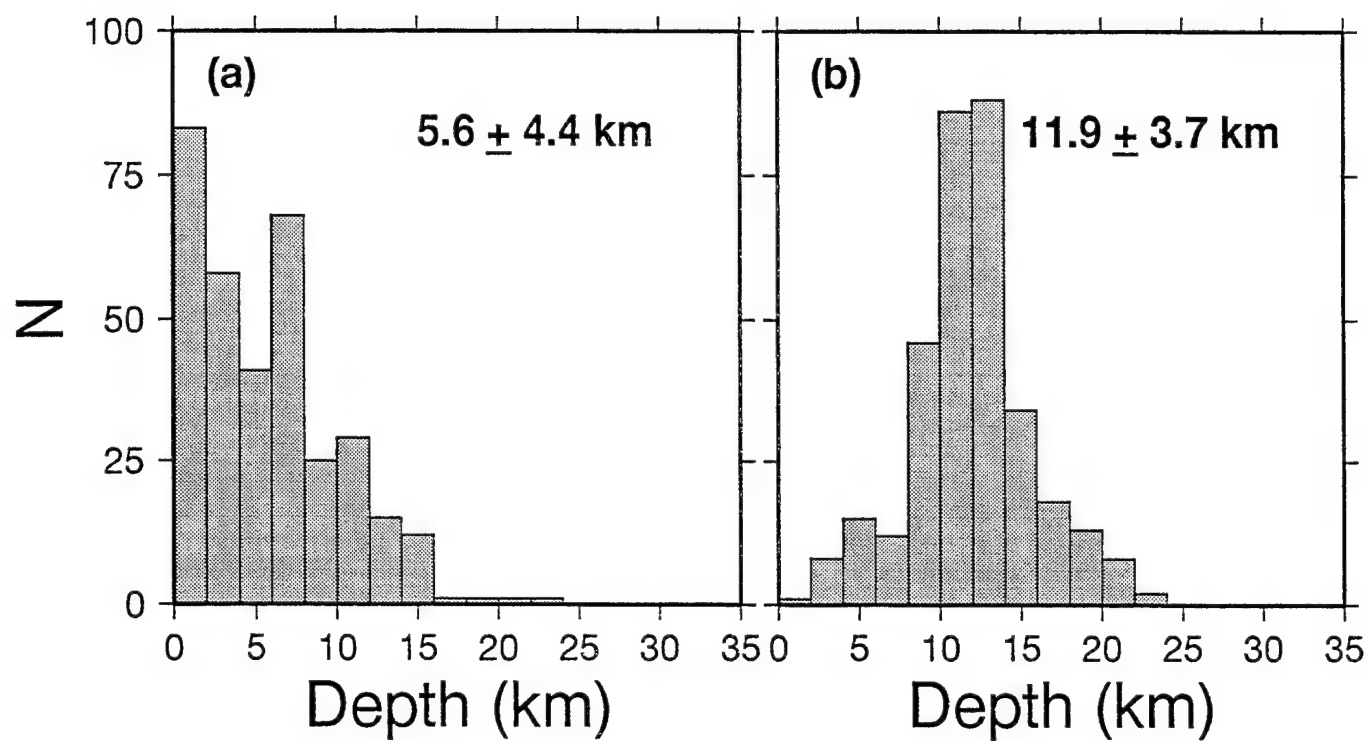


Figure 14

With the advent of broadband instrumentation, it is possible to make some useful estimates of the energy levels of sources. This is especially attractive at local and regional distances before the strong attenuation of the upper mantle has stripped away the higher frequencies. However, we must be able to correct for the strong propagational effects produced by the crust before obtaining accurate energy estimates.

We proceed by making some useful definitions in terms of a source time history needed to make definitive broadband moment estimates. Because energy depends on velocity, we must be careful in defining the time history, especially at the highest frequency. The approach followed here is to base this estimate on the P_{nl} window which we think is the least contaminated by the complex surface layer. Since the WASP records are difficult to match in waveform, we choose to base the time history on that triangle, dt_i , which best predicts the energy ratio of synthetic (WASP/LP) to that of the observations. The broadband moment (M_B) is defined as the best fitting synthetic to the observed data assuming this time history with the orientation parameters determined by the long-period fit.

In the same fashion as M_B we define the energy moment, M_E , to be the ratio of the total integrated broadband energy (3 components) divided by the corresponding integrated Green's functions. To be more specific we will write down the explicit expressions for the tangential component, we define

$$M = V_{obs}(t) / V_g(t) \quad (6)$$

where

M = moment

$V_g(t)$ = synthetic for a particular far-field source history, $\dot{D}(t)$

$V_{obs}(t)$ = observed record We define $M = M_0$ when these amplitude comparisons are performed at long-periods, and M_B when performed with the $\dot{D}(t)$ fixed by the (SPZ/LP) ratio. The energy strength is defined by

$$M_E = \left[\int_0^T \dot{V}_{obs}^2(t) dt / \int_0^T \dot{V}_g^2(t) dt \right]^{1/2} \quad (7)$$

where T is the length of the records. This same procedure is applied to all components and averaged to define the M 's for a particular event. If the synthetics fit the observed data exactly, we would obtain M_E equal to M_B or a ratio (M_E/M_B) of 1.

Applying this formalism to the Little Skull Mountain main event we obtain broadband fits nearly identical to those in Figure 8. We obtain a time history given by $\delta t_i = 0.3$ secs. The corresponding short-period comparisons of synthetics with observations are displayed in Figure 15. These comparisons are quite good and are typical of results from other events, see Zhao and Helmberger (1996).

We do not want definitions of source properties such as moment and energy to depend on the range or receiver. Thus, we can check the usefulness of our definitions by plotting (M_E/M_B) as a function of distance and model as in Figure 16. Most of the points fall between .5 and 1.5. This plot shows no obvious distance dependence suggesting that our path corrections are adequate. However, there is a slight baseline shift with the PB model yielding slightly higher values. But in general, the various moments and source parameter appear to be quite independent of model if we treat deep sources, i.e., $d > 5$ km. Note that the more detailed the upper portion of the model becomes, the more likely it will become path dependent. If we want to use the same model for a large region, we want to keep the model simple and restrict the source depths accordingly.

With this brief review of source estimation, we return to the observations displayed in Figure 2. Note that while the peak short-period (SP) amplitudes are similar, the long-period outputs are an order-of-magnitude different. This comparison is typical (Woods *et al.*, 1993). Also, note that the explosion data contains many more arrivals or energy than do the earthquake traces. Therefore, if we simply compare the ratio of (M_E/M_B) , we should distinguish the two types of events. But to do this, we must first obtain estimates of M_O , M_B , and M_E from explosions. We do this by assuming all events are earthquakes or double-couple's. An example calculation is given in Figure 17.

In this match of synthetics to observations, we have used the (WASP/WALP) ratio to fit the time history because of the noise in the LP bandpass. A value of (.1,.1) triangle was obtained. While the short-period details are not well explained, the overall estimate of long-period waveform fits is reasonable. We obtain a moment of 1.1×10^{22} dyne-cm and a source orientation of $(220^\circ, 30^\circ, 115^\circ)$ for strike, dip, and rake. The source depth search preferred the depth of 5 km which is the shallowest depth allowed. Woods *et al.* (1993) obtained a $M_O = 3 \times 10^{21}$ dyne-cm for this event or about 4 times smaller than the above estimate. This difference is expected because of the relative strengths of Rayleigh wave Green's functions for two reasons. First, since the excitation of Rayleigh waves per unit of moment is stronger at the shallower depth, we can understand why a larger moment is needed to fit the data assuming a depth of 5 km. Second, since the radiation pattern for an earthquake is always less than for an explosion, we again require an increased moment to compensate. The M_B moment is obtained by

matching the amplitudes in the upper two plots yielding $.5 \times 10^{22}$ dyne-cm, which is lower than M_0 . This is caused by the short-period spikes riding on top of the observed Rayleigh waves; something which does not occur in the synthetics but holds true for most observations of explosions. Thus, the M_B measure from explosions is not a very good measure of source strength since it appears to be affected by these short-period spikes. The M_E measure is also strongly affected by these spikes and decreased accordingly. However, the extra arrivals occurring in the observations increase M_E , yielding $M_E = 1.2 \times 10^{22}$ dyne-cm or a ratio of $M_E/M_B = 2.3$. Earthquakes yield values near unity as discussed above, thus it is an effective depth discriminant. Figure 18 shows the results for NTS explosions and southwestern U. S. earthquakes. Each point represents one event.

A more empirical approach is to use the short-period:long-period (SP:LP) ratio. The source properties that we want to quantify are the short-period (1 Hz) P-wave and long-period (0.14 to 0.05 Hz) surface wave energy levels, the ratio of which is used as the discrimination criterion. The short-period bandpass is the same used to measure teleseismic P-wave amplitudes for the $m_b:M_s$ discriminant. The long-period bandpass represents the predominant frequency range of the fundamental-mode Airy Phase at regional distances (Alewine, 1972). This short-period vs. long-period energy ratio ($ESP:LP$) is defined as:

$$E_{SP:LP} = \frac{\int_{t_{pn}}^{t_{sn}} v_{sp}(t)^2 dt}{\sum_{i=1}^3 \int_{t_1}^{t_2} v_{lp}(t)^2 dt}, \quad (8)$$

with the summation being for the three components and t_i representing the windowing times determined from travel path length and the wave train of interest; t_{pn} corresponds to the time before the onset of the P-wave and t_{sn} the time prior to the S-wave onset time, and t_1 and t_2 bracket the time window of the fundamental Rayleigh and Love waves. v_{sp} and v_{lp} are the short-period and long-period ground bandpass velocities, respectively. v_{sp} is obtained by convolving the broadband velocity record convolved with a Wood-Anderson (WA) short-period instrument and v_{lp} is the broadband velocity record convolved with a long-period instrument (PE). The velocities are squared in order to obtain units of energy; the factor of $m/2$ in the numerator and denominator, where m is the unit mass of the particle of motion, cancel out.

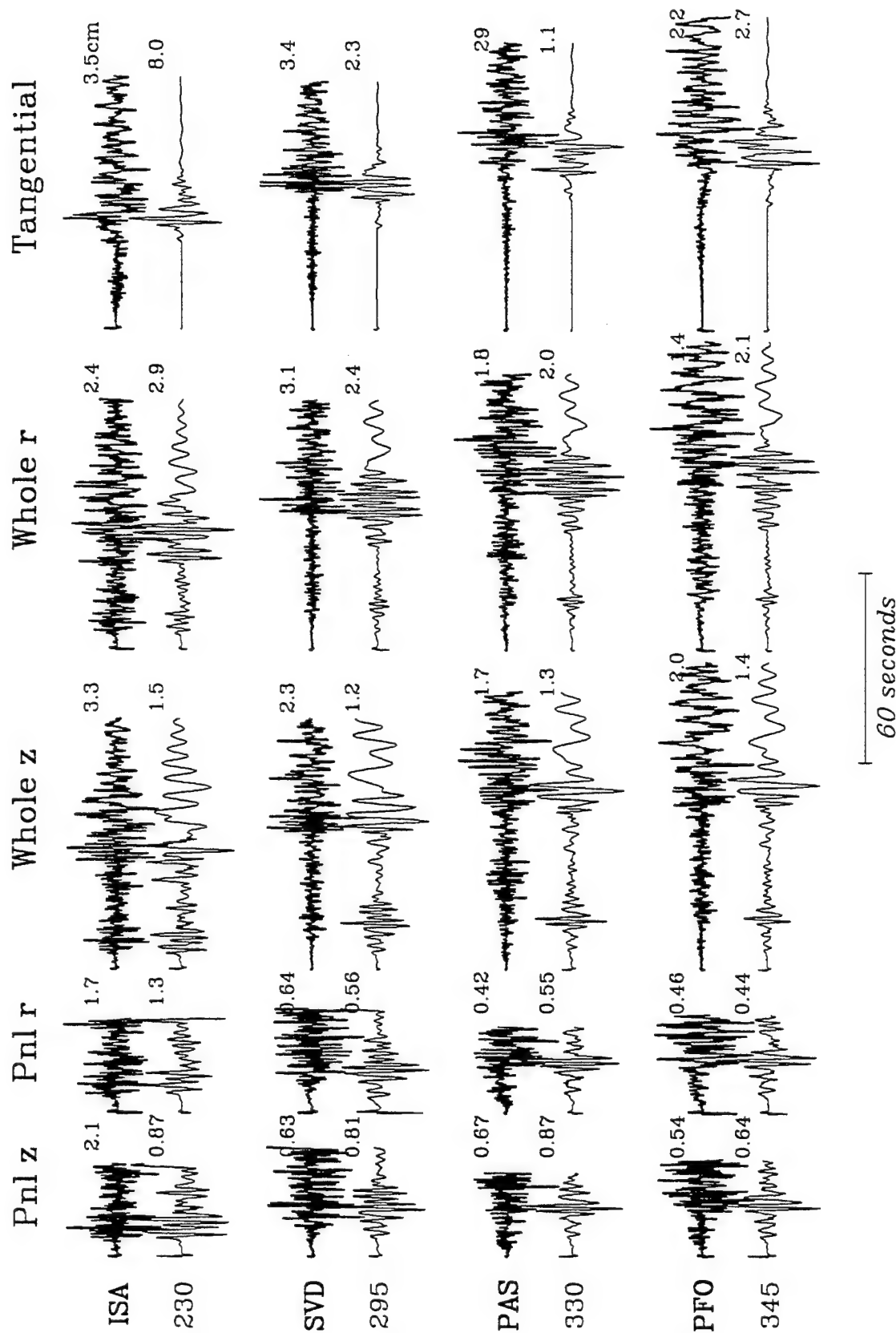


Figure 15

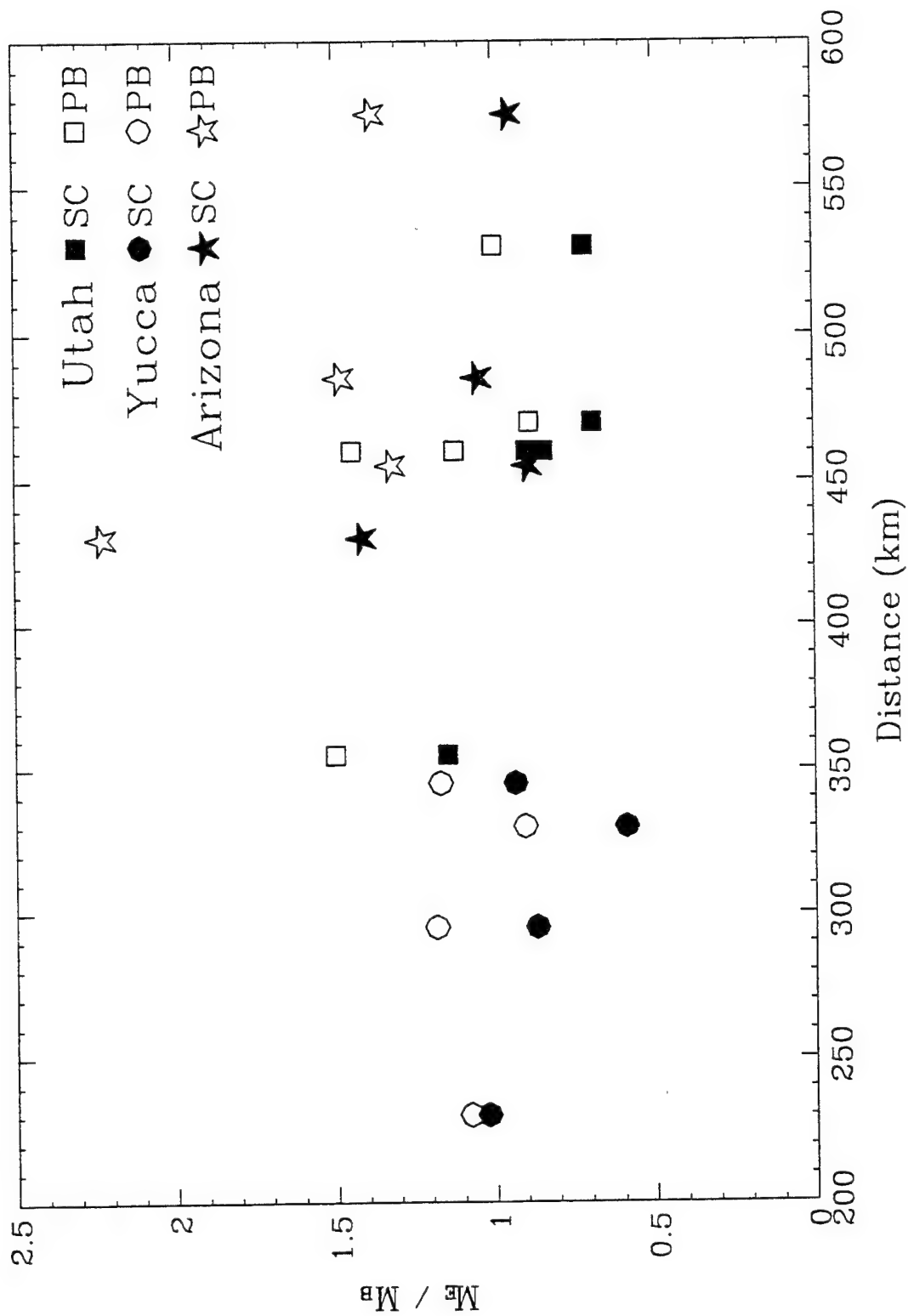


Figure 16

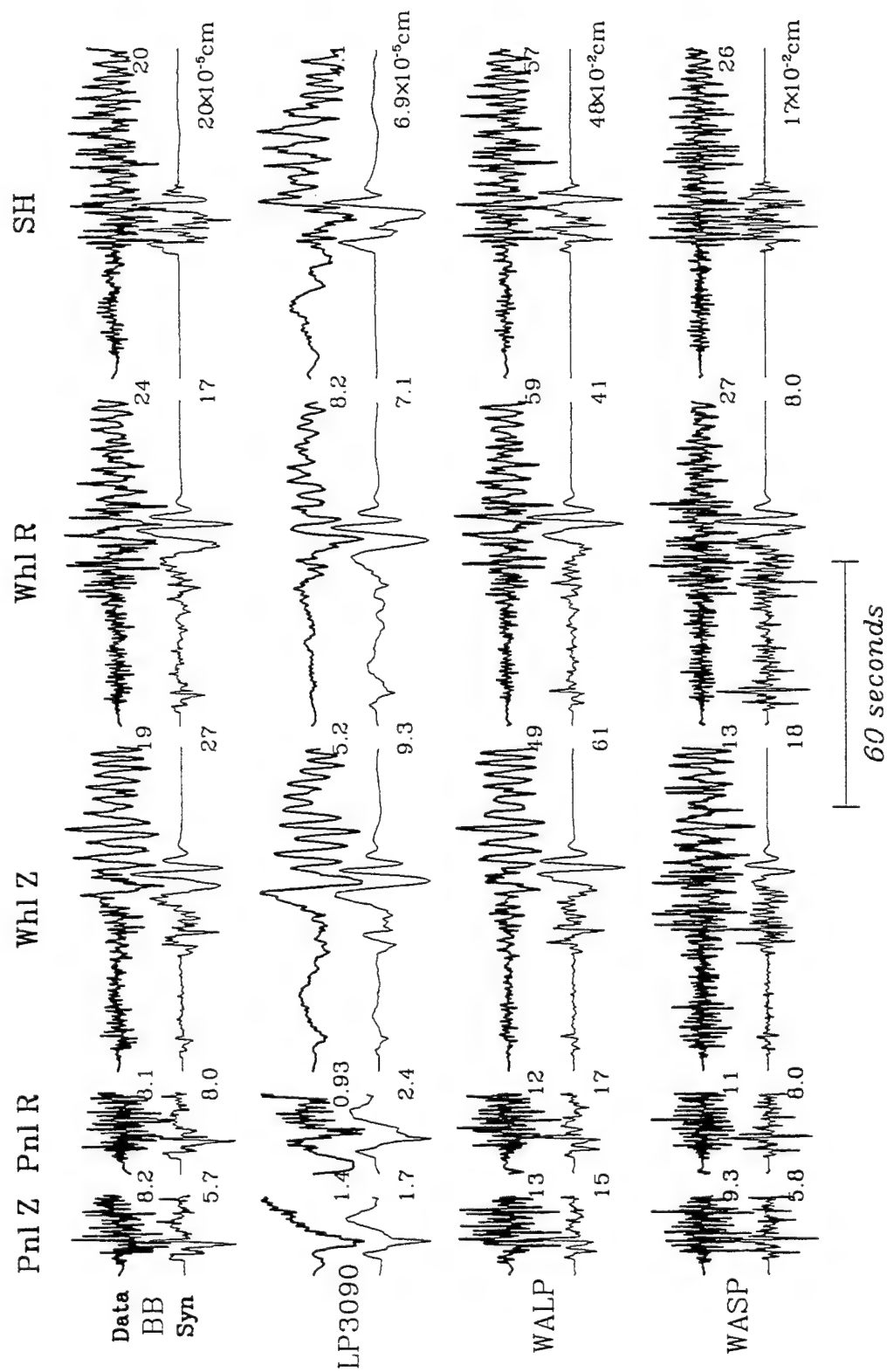


Figure 17

Figure 19 displays the log SP:LP integrated energy ratio vs. distance for all data; each data point represents one event-station pair. Crosses represent earthquakes, circles signify nuclear explosions, and stars are data points for the chemical kt test. The explosions tend to have higher SP:LP integrated energy ratios than do the earthquakes at all distance ranges. Although there isn't complete separation of the two populations, the portion of the earthquake population which overlaps with the explosion population is small (approximately 10 percent).

6. Discussion

In order to better appreciate the robustness of these energy measurements and their application to particularly small events, we will show a suite of regional waveforms and their associated integrated energy curves for small explosions from the three NTS subsites and for earthquakes near NTS, namely the Little Skull Mountain sequence. We will also briefly discuss Northridge observations displaying some obvious scattering effects produced by surface geology.

As noted earlier, NTS records are in sharp contrast to natural earthquake records as displayed in Figure 2 where the onset of shear waves is quite clear. These recordings are at fairly near distances so that propagation effects are minimized. However, these characteristics persist to larger ranges, Woods and Helmberger (1996). These waveform characteristics are displayed in the integrated energy curves as well.

The panel on the left in Figure 20 displays the short-period, vertical component, integrated energy curves vs. time for explosions recorded at the four TERRAScope stations. All curves are normalized to unity, with the actual integrated energy value given to the right in the legend. We will refer to these plots as $E(t)$, or accumulated energy up to time t . For records with a prominent P-wavetrain arrival, the curves resemble step functions. This is particularly true of the Pahute shot and expected on theoretical grounds, i.e., RDP source. For the Yucca shot, the P-wavetrain energy comprises less than half of the short-period energy. The Rainier nuclear explosion and chemical blast are intermediate in shape to the Pahute and Yucca energy curves. At the more distant stations (PAS and PFO), the Rainier energy curves more closely resemble those of Yucca than Pahute, whereas at the closer stations, particularly ISA, the opposite is true.

The panel on the right in Figure 20 displays analogous plots of integrated energy curves for earthquakes from the Little Skull Mountain sequence. Here the onset of the S-wave energy is pronounced and sharp. For explosions, in general, the S-wave onset is much more gradual, with the exception of the Yucca event recorded at PFO, which looks very much like the earthquake energy curves. It is not clear whether these differences are

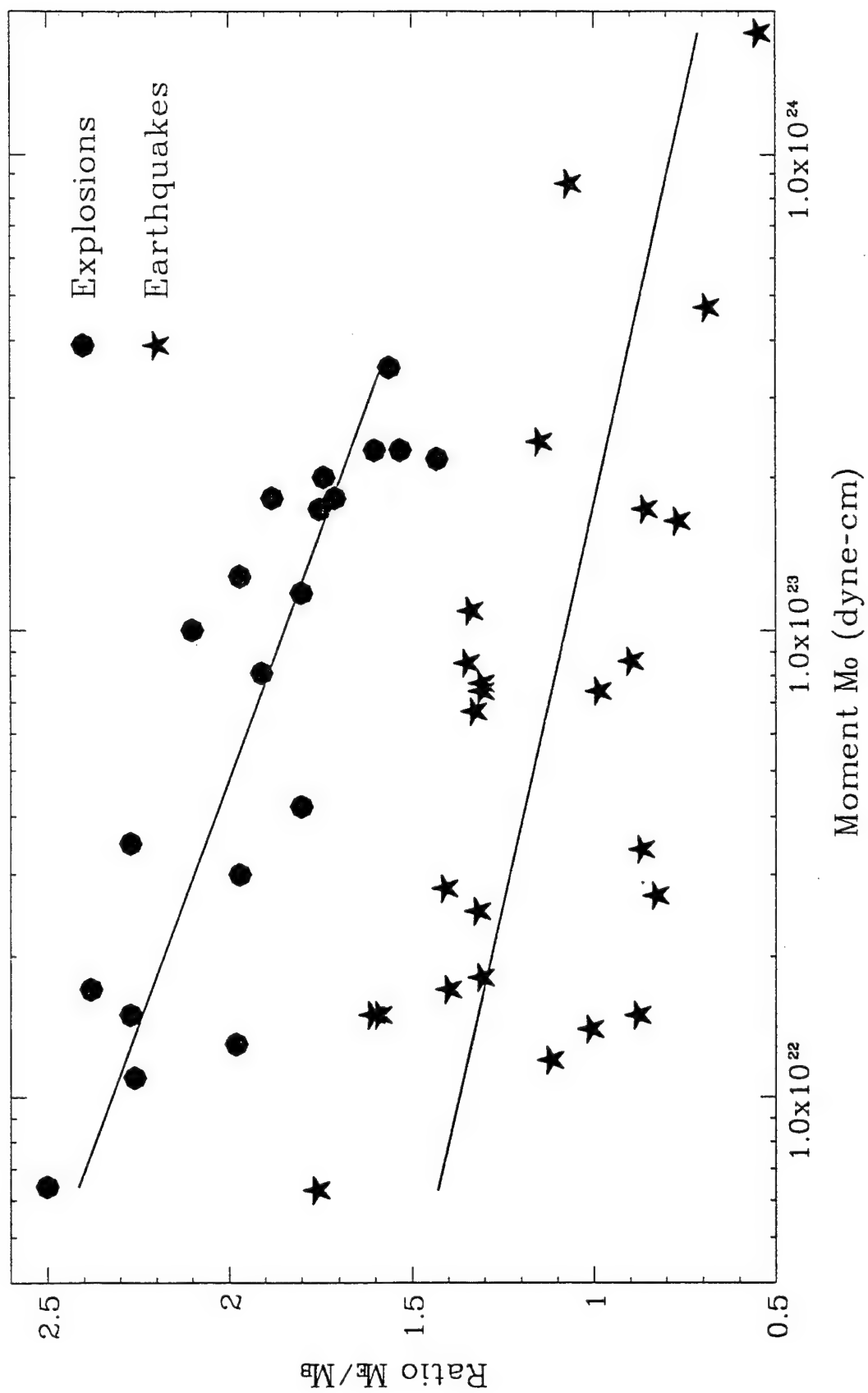


Figure 18

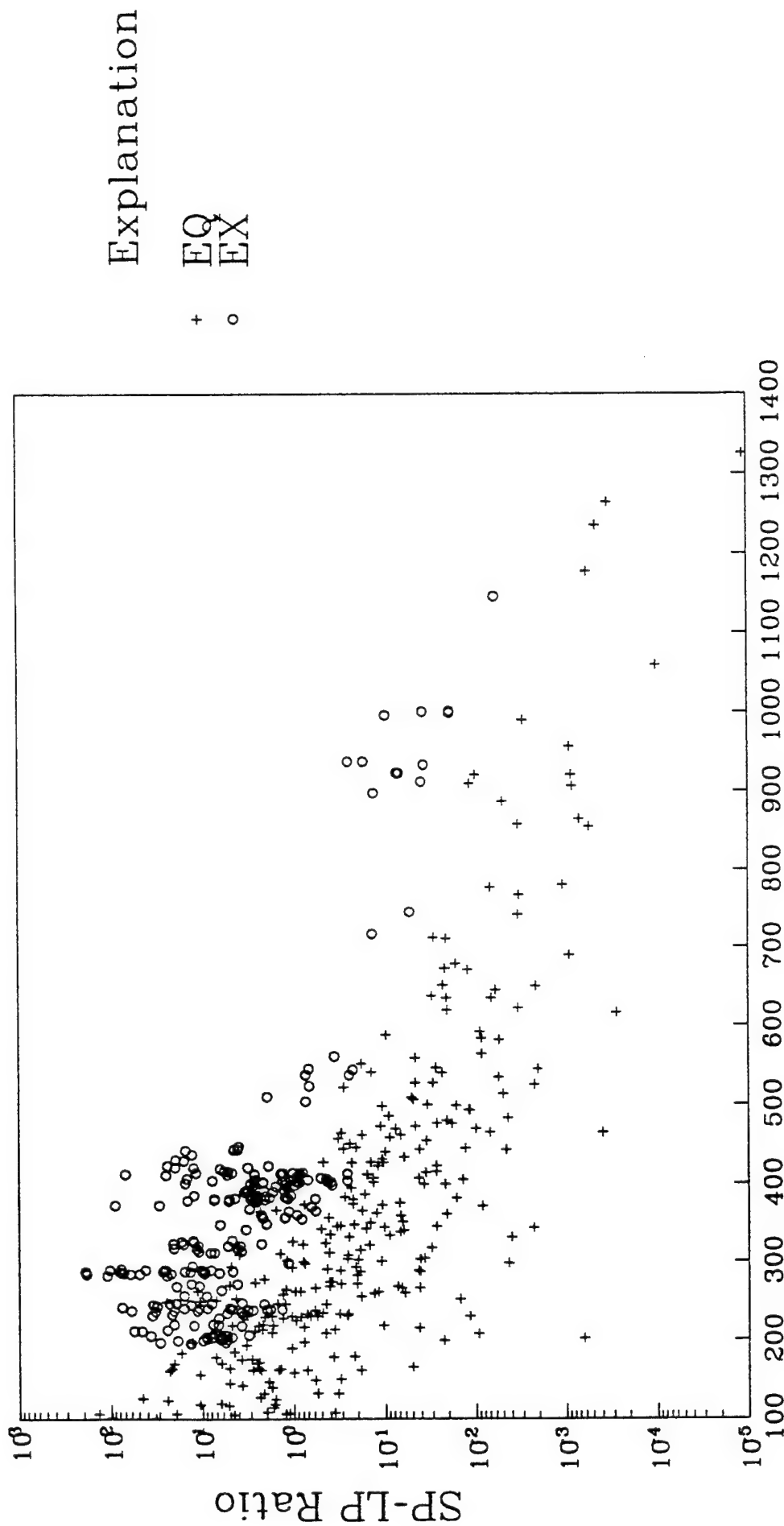
due to near-source or propagation effects. In the case of Yucca Flat for which the energy curve at each station deviates significantly from the "cleaner" Pahute curve, it seems likely that shallow structure in the source region is at least partly responsible for the large amount of scattered energy in the waveforms.

Several investigations have discussed the scattering of locally trapped Rayleigh waves encountering NTS type structures, see for example, McLaughlin and Jih (1987), and Stead and Helmberger (1988). However, explaining all three components of regional NTS events (Figure 3) proves especially difficult because of the amount of tangential energy generally observed. Thus, the scattering must be due to a 3-D feature and/or requires secondary sources such as spall, etc. In short, it is difficult to predict regional records using the conventional RDP formalism.

An easier problem that has been studied quite successfully involves modeling events occurring along a corridor from Imperial Valley to Pasadena, essentially events on the San Jacinto fault zone, see Helmberger *et al.* (1992), and Ho and Helmberger (1989). Events occurring in the Imperial Valley arrive at Pasadena with extensive coda compared to events occurring outside the basin, see Figure 21. The upper panel displays a 2-D model connecting Imperial Valley to Pasadena (260 km). The (AN) event occurred near the edge while the (IV) event is located well into the basin. Basin events not only have well developed dispersion but many times have secondary arrivals. The shallower the event, the stronger these later arrivals. These signals can be modeled as shallow surface waves propagating slowly in the upper layer and re-radiating at the basin edge, and can be the strongest signals on the record if the source extends to the surface, see Ho and Helmberger (1989). Thus, it is relatively easy to explain the excess energy associated with shallow events occurring in soft materials from a theoretical point-of-view.

The same features observed from the Imperial Valley events can be seen in the Northridge data, Song and Helmberger (1996). As an example of this complexity, we compare the vertical broadband and short-period displacement data and cumulative energy curves for stations GSC and PFO, for 3 earthquakes at different depths (Figure 22). These three events occurred under the Santa Susana Mountains within 10 km of each other. Note the difference in the Rayleigh wavetrain between the records at GSC and PFO for the various event. Energy arrives at station GSC in a time window narrower than at station PFO. These features also show up on the short-period records. As the source gets deeper, this difference becomes less significant. Scattering due to the more heterogeneous structure from Northridge to PFO would be one reason for this difference. Note that the path from Northridge to station GSC is relatively uniform and mainly a hard rock path. Path to PFO passes through the San Fernando basin and part of the Los

SP-LP(3-comp) Ratio vs. Distance



Distance (Km)

Figure 19

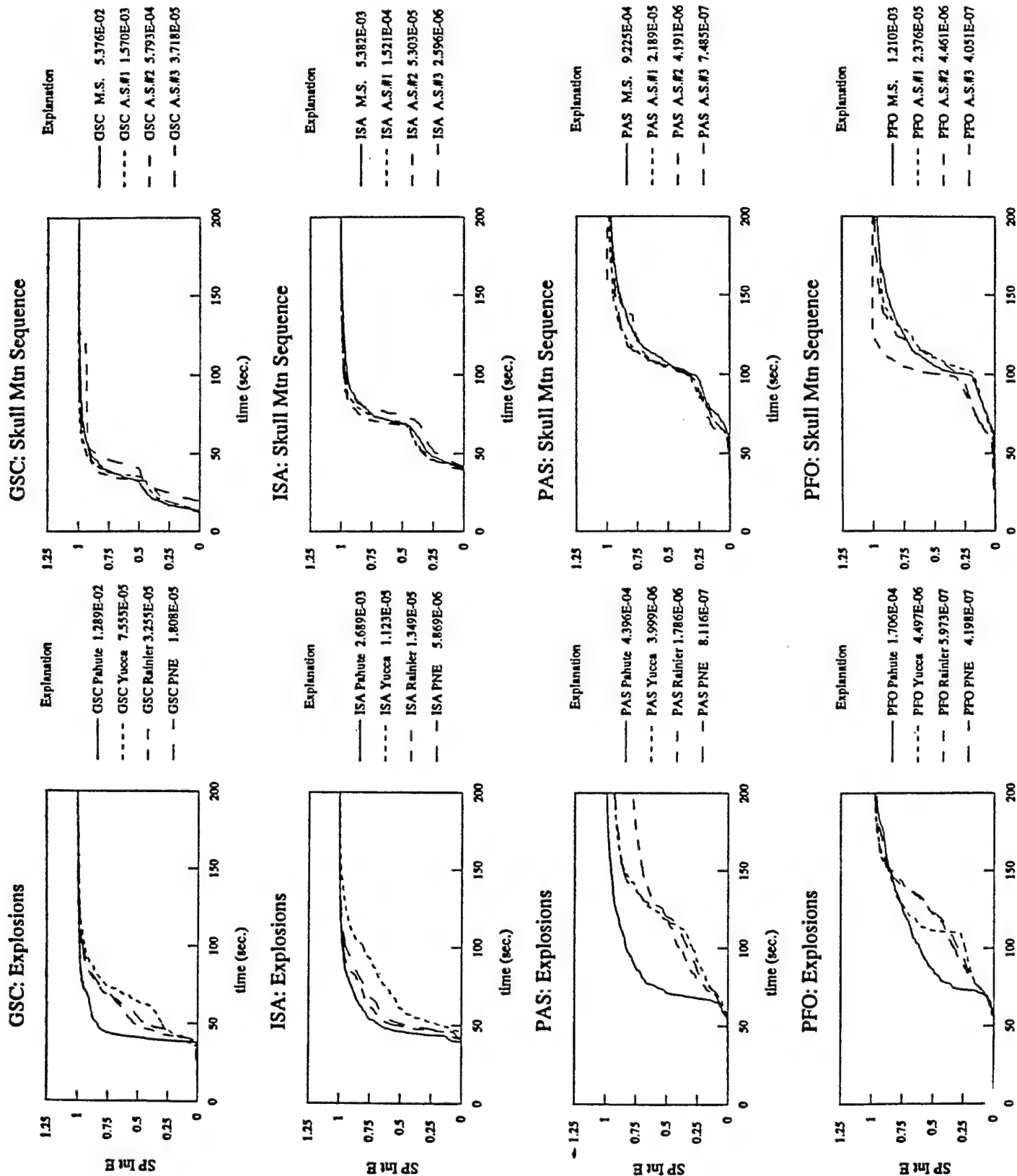


Figure 20

Angeles basin. Another factor that might explain the above difference is the basin effect. For the shallow earthquake, part of the surface wave energy is trapped in the basin and propagates along the top slow layer. This forms the extend Rayleigh wavetrain when it arrives at station PFO. Thus energy arriving at PFO along different paths spreads out in a wider time window, see Song and Helmberger (1996).

Applying this experience to the NTS data, we suggest that the Yucca Flat basin is responsible for the complicated records and that natural earthquakes, which normally occur at deeper depths, are generally easier to model. Thus, the similarity in wave shapes and energy curves allows us to model the large earthquake ($M > 5$) where the signals are above the noise, identify the paths of short-period arrivals and predict their behavior for small events. In short, we think it is easier to understand the short-period phases produced by the Little Skull Mountain events than those produced by the NTS shots. Thus, we propose to identify earthquakes by their wave shapes and energy distributions and identify explosions as being not-like-earthquakes.

In conclusion, we demonstrated that regional seismograms from earthquakes can be used to estimate their fault parameters, moment, and depths applying a procedure developed in Zhao and Helmberger (1994) and extended by Zhu and Helmberger (1996). Next we examined the energy content of the various phases, defined M_B (broadband moment) and M_E (energy strength), and introduced a new method of discrimination. In this method all events are processed as earthquakes, and explosions are distinguished by their stronger energy levels relative to their long-period amplitudes. This was followed by a discussion of a discriminant based on the ratio of short-period (1 Hz), vertical component, P_{nl} wavetrain energy to intermediate-period (0.05 to 0.16 Hz), three component, surface wave energy, for which explosions tend to have a higher ratio than earthquakes. This discriminant works on the same premise as the teleseismic $M_S:m_b$ ratio, for which earthquakes are richer in long-period surface wave energy relative to explosions.

7. Acknowledgments.

We thank Evelina Cui and Dee Page for their efforts in producing this report. This research was supported by the Department of Defense as monitored by the Air Force Office of Scientific Research under Contract F19628-95-C-0095.

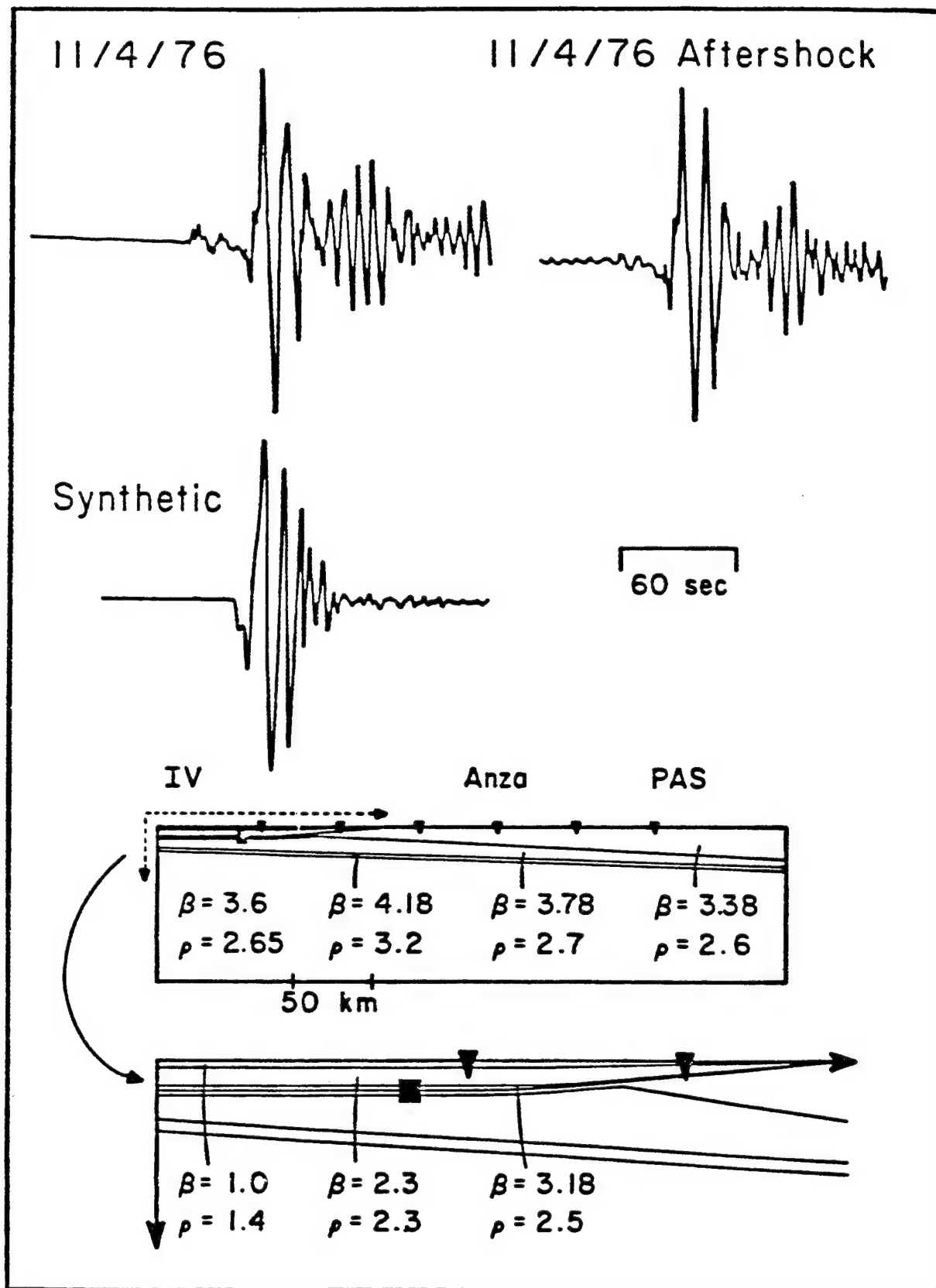


Figure 21

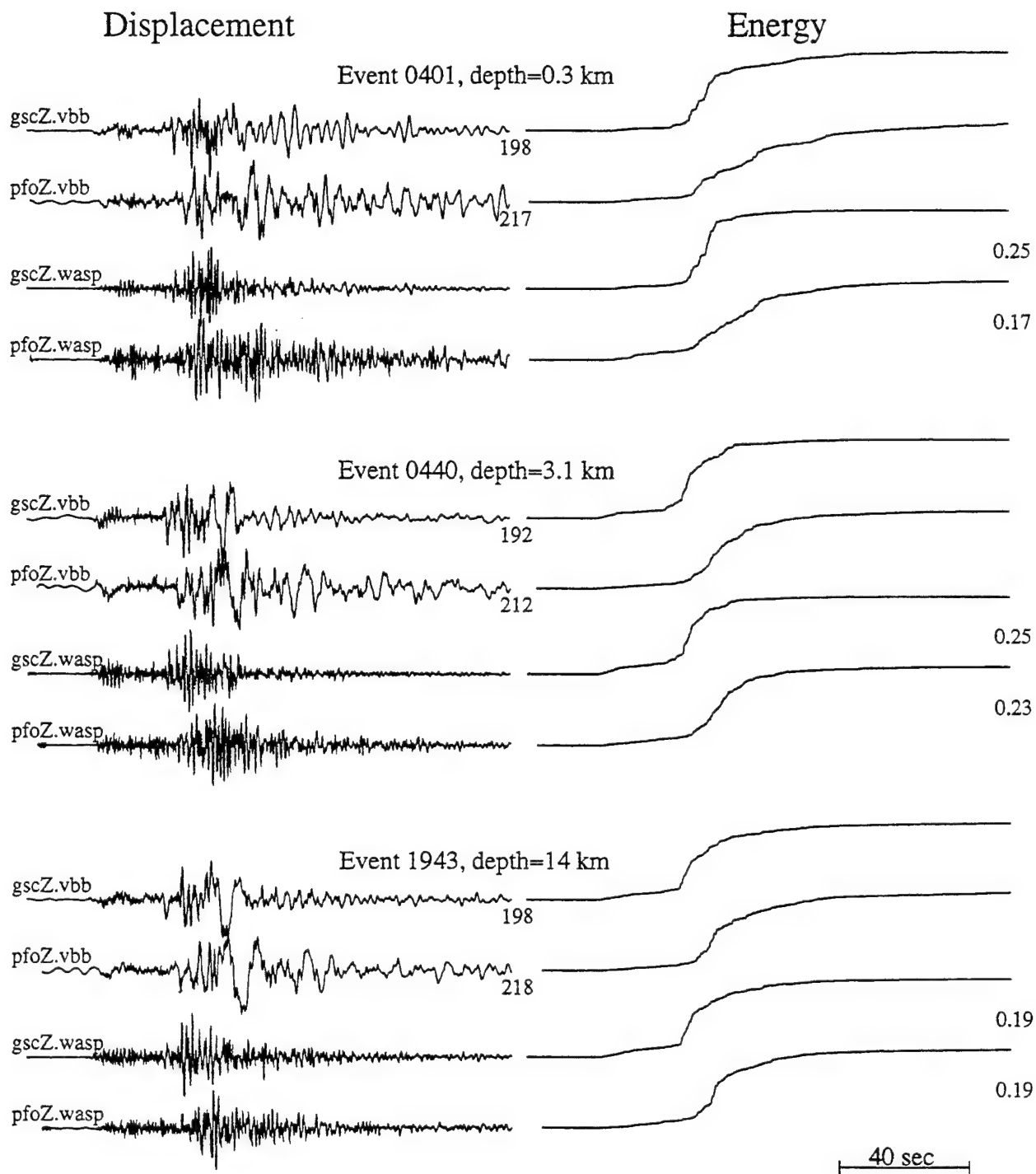


Figure 22

8. References

- Alewine, R. W. (1972) Theoretical and observed distance corrections for Rayleigh-Wave magnitude, *Bull. Seismol. Soc. Am.* **62**, no. 6, 1611-1619.
- Doser, D. I and H. Kanamori (1986) Depth of seismicity in the Imperial Valley region 1977-1983 and its relationship to heat flow, crustal structure, and the October 15, 1979 earthquake, *J. Geophys. Res.* **91**, 675-688.
- Dreger, D. S. and Helmberger, D. V. (1991) Source parameters of the Sierra Madre earthquake from regional and local body waves, *Geophys. Res. Lett.* **18**, 2015-2018.
- Dreger, D. S. and Helmberger, D. V. (1993) Determination of source parameters at regional distances with three-component sparse network data, *J. Geophys. Res.* **98**, B5, 8107-8125.
- Dziewonski, A. M. and Anderson, D. L. (1981) Preliminary reference Earth model, *Phys. Earth Planet. Inter.* **25**, 297-356.
- Fan, G. W., S. L. Beck, and T. C. Wallace (1994) The seismic source parameters of the 1991 Costa Rica aftershock sequence: Evidence for a transcurrent plate boundary, *J. Geophys. Res.* **98**, 15759-15778.
- Helmberger, D., R. Stead, P. Ho-Liu and D. Dreger (1992) Broadband modeling of regional seismograms: Imperial Valley to Pasadena, *Geophys. J. Int.* **110**, 42-54.
- Ho-Liu, P. and D. V. Helmberger (1989) Modeling regional Love waves: Imperial Valley to Pasadena, *Bull. Seismol. Soc. Am.* **79**, 1194-1209.
- Marone, C. and C. H. Scholz (1988) The depth of seismic faulting and the upper transition from stable to unstable slip regimes, *Geophys. Res. Lett.* **15**, 621-624.
- Meissner, R. and J. Strehlau (1982) Limits of stresses in continental crust and their relationship to the depth-frequency distribution of shallow earthquakes, *Tectonics* **1**, 73-89.
- McLaughlin, K. L. and Jih, R.-S. (1987) Finite-difference simulations of Rayleigh wave scattering by shallow heterogeneity, *Report AFGL-TR-87-0322*, Air Force Geophysics Laboratory, Hanscom AFB, MA, ADA194961.
- Patton, H. J. and Walter, W. R. (1993) Regional moment: magnitude relations for earthquakes and explosions, *Geophys. Res. Lett.* **20**, 277-280.
- Patton, H. J. and Zandt, G. (1991) Seismic moment tensors of western U. S. earthquakes and implications for the tectonic stress field, *J. Geophys. Res.* **96**, 18,245-18,259.
- Priestley, K. and Brune, J. (1978) Surface waves and the structure of the Great Basin of Nevada and western Utah, *J. Geophys. Res.* **83**, 2,265-2,276.
- Ritsema, J. and Lay, T. (1994) Rapid source mechanism determination of large ($M_w \geq 5$) earthquakes in the western United States, *Geophys. Res. Lett.* **20**, 1611-1614.

- Sibson, R. (1984) Roughness at the base of the seismogenic zone: contributing factors, *J. Geophys. Res.* **89**, 5791-5799.
- Song, X. J. and D. V. Helmberger (1996) The Northridge aftershocks, a source study with TERRAscope data, submitted to *Geophys. J. Int.*
- Stead, R. J. and Helmberger, D. V. (1988) Numerical-analytical interfacing in two dimensions with applications to modeling NTS seismograms, *PAGEOPH* **128**, 157-193.
- Taylor, S. R., Denney, M. D., Vergino, E. S., and Glaser, R. E. (1989) Regional discrimination between NTS explosions and western U. S. Earthquakes, *Bull. Seismol. Soc. Am.* **79**, 1142-1176.
- Thio, H. K. and Kanamori, H. (1992) Moment tensor inversions in Southern California using surface waves recorded by TERRAscope, (abstract), *EOS Trans., AGU* **73**, 376.
- Wallace, T. C. and D. V. Helmberger (1982) Determination of seismic parameters of moderate-size earthquake from regional waveforms, *Phys. E-Plan.* **30**, 185-196.
- Woods, B. and Helmberger, D. V. (1996) Regional seismic discriminants using wavetrain energy ratios, submitted to *Bull. Seismol. Soc. Am.*
- Woods, B., Kedar, S., and Helmberger, D. V. (1993) $M_L:M_0$ as a regional seismic discriminant, *Bull. Seismol. Soc. Am.* **83**, 1167-1183.
- Woods, B. and Harkrider, D. G. (1994) Investigating long-period source spectra of Nevada Test Site explosions using regional surface wave data with applications to yield estimation and discrimination, *Geophys. J. Int.* (in press).
- Zhao, L. S. and Helmberger, D. V. (1994) Source estimation from broadband regional seismograms, *Bull. Seismol. Soc. Am.* **84**, 91-104.
- Zhao, L. S. and Helmberger, D. V. (1994) Regional moments, energy levels, and a new discriminant, submitted to *Phys. Earth Planet. Inter.*
- Zhu, L., and Helmberger, D. V. (1996). Advancement in source estimation techniques using broadband regional seismograms, submitted to *Bull. Seismol. Soc. Am.*

THOMAS AHRENS
SEISMOLOGICAL LABORATORY 252-21
CALIFORNIA INSTITUTE OF TECHNOLOGY
PASADENA, CA 91125

RALPH ALEWINE
NTPO
1901 N. MOORE STREET, SUITE 609
ARLINGTON, VA 22209

SHELTON ALEXANDER
PENNSYLVANIA STATE UNIVERSITY
DEPARTMENT OF GEOSCIENCES
537 DEIKE BUILDING
UNIVERSITY PARK, PA 16801

MUAWIA BARAZANGI
INSTITUTE FOR THE STUDY OF THE CONTINENTS
3126 SNEE HALL
CORNELL UNIVERSITY
ITHACA, NY 14853

RICHARD BARDZELL
ACIS
DCI/ACIS
WASHINGTON, DC 20505

T.G. BARKER
MAXWELL TECHNOLOGIES
P.O. BOX 23558
SAN DIEGO, CA 92123

DOUGLAS BAUMGARDT
ENSCO INC.
5400 PORT ROYAL ROAD
SPRINGFIELD, VA 22151

THERON J. BENNETT
MAXWELL TECHNOLOGIES
11800 SUNRISE VALLEY DRIVE SUITE 1212
RESTON, VA 22091

WILLIAM BENSON
NAS/COS
ROOM HA372
2001 WISCONSIN AVE. NW
WASHINGTON, DC 20007

JONATHAN BERGER
UNIVERSITY OF CA, SAN DIEGO
SCRIPPS INSTITUTION OF OCEANOGRAPHY IGPP, 0225
9500 GILMAN DRIVE
LA JOLLA, CA 92093-0225

ROBERT BLANDFORD
AFTAC
1300 N. 17TH STREET
SUITE 1450
ARLINGTON, VA 22209-2308

STEVEN BRATT
NTPO
1901 N. MOORE STREET, SUITE 609
ARLINGTON, VA 22209

RHETT BUTLER
IRIS
1616 N. FORT MEYER DRIVE
SUITE 1050
ARLINGTON, VA 22209

LESLIE A. CASEY
DOE
1000 INDEPENDENCE AVE. SW
NN-40
WASHINGTON, DC 20585-0420

CATHERINE DE GROOT-HEDLIN
SCRIPPS INSTITUTION OF OCEANOGRAPHY
UNIVERSITY OF CALIFORNIA, SAN DIEGO
INSTITUTE OF GEOPHYSICS AND PLANETARY PHYSICS
LA JOLLA, CA 92093

STANLEY DICKINSON
AFOSR
110 DUNCAN AVENUE, SUITE B115
BOLLING AFB
WASHINGTON, D.C. 20332-001

SEAN DORAN
ACIS
DCI/ACIS
WASHINGTON, DC 20505

DIANE I. DOSER
DEPARTMENT OF GEOLOGICAL SCIENCES
THE UNIVERSITY OF TEXAS AT EL PASO
EL PASO, TX 79968

RICHARD J. FANTEL
BUREAU OF MINES
DEPT OF INTERIOR, BLDG 20
DENVER FEDERAL CENTER
DENVER, CO 80225

JOHN FILSON
ACIS/TMG/NTT
ROOM 6T11 NHB
WASHINGTON, DC 20505

MARK D. FISK
MISSION RESEARCH CORPORATION
735 STATE STREET
P.O. DRAWER 719
SANTA BARBARA, CA 93102-0719

LORI GRANT
MULTIMAX, INC.
311C FOREST AVE. SUITE 3
PACIFIC GROVE, CA 93950

I. N. GUPTA
MULTIMAX, INC.
1441 MCCORMICK DRIVE
LARGO, MD 20774

JAMES HAYES
NSF
4201 WILSON BLVD., ROOM 785
ARLINGTON, VA 22230

MICHAEL HEDLIN
UNIVERSITY OF CALIFORNIA, SAN DIEGO
SCRIPPS INSTITUTION OF OCEANOGRAPHY IGPP, 0225
9500 GILMAN DRIVE
LA JOLLA, CA 92093-0225

EUGENE HERRIN
SOUTHERN METHODIST UNIVERSITY
DEPARTMENT OF GEOLOGICAL SCIENCES
DALLAS, TX 75275-0395

VINDELL HSU
HQ/AFTAC/TTR
1030 S. HIGHWAY A1A
PATRICK AFB, FL 32925-3002

RONG-SONG JIH
PHILLIPS LABORATORY
EARTH SCIENCES DIVISION
29 RANDOLPH ROAD
HANSCOM AFB, MA 01731-3010

LAWRENCE LIVERMORE NATIONAL LABORATORY
ATTN: TECHNICAL STAFF (PLS ROUTE)
PO BOX 808, MS L-200
LIVERMORE, CA 94551

LAWRENCE LIVERMORE NATIONAL LABORATORY
ATTN: TECHNICAL STAFF (PLS ROUTE)
PO BOX 808, MS L-221
LIVERMORE, CA 94551

ROBERT GEIL
DOE
PALAIS DES NATIONS, RM D615
GENEVA 10, SWITZERLAND

HENRY GRAY
SMU STATISTICS DEPARTMENT
P.O. BOX 750302
DALLAS, TX 75275-0302

DAVID HARKRIDER
PHILLIPS LABORATORY
EARTH SCIENCES DIVISION
29 RANDOLPH ROAD
HANSCOM AFB, MA 01731-3010

THOMAS HEARN
NEW MEXICO STATE UNIVERSITY
DEPARTMENT OF PHYSICS
LAS CRUCES, NM 88003

DONALD HELMBERGER
CALIFORNIA INSTITUTE OF TECHNOLOGY
DIVISION OF GEOLOGICAL & PLANETARY SCIENCES
SEISMOLOGICAL LABORATORY
PASADENA, CA 91125

ROBERT HERRMANN
ST. LOUIS UNIVERSITY
DEPARTMENT OF EARTH & ATMOSPHERIC SCIENCES
3507 LACLEDE AVENUE
ST. LOUIS, MO 63103

ANTHONY IANNACCHIONE
BUREAU OF MINES
COCHRANE MILL ROAD
PO BOX 18070
PITTSBURGH, PA 15236-9986

THOMAS JORDAN
MASSACHUSETTS INSTITUTE OF TECHNOLOGY
EARTH, ATMOSPHERIC & PLANETARY SCIENCES
77 MASSACHUSETTS AVENUE, 54-918
CAMBRIDGE, MA 02139

LAWRENCE LIVERMORE NATIONAL LABORATORY
ATTN: TECHNICAL STAFF (PLS ROUTE)
PO BOX 808, MS L-207
LIVERMORE, CA 94551

LAWRENCE LIVERMORE NATIONAL LABORATORY
ATTN: TECHNICAL STAFF (PLS ROUTE)
LLNL
PO BOX 808, MS L-175
LIVERMORE, CA 94551

LAWRENCE LIVERMORE NATIONAL LABORATORY
ATTN: TECHNICAL STAFF (PLS ROUTE)
PO BOX 808, MS L-208
LIVERMORE, CA 94551

LAWRENCE LIVERMORE NATIONAL LABORATORY
ATTN: TECHNICAL STAFF (PLS ROUTE)
PO BOX 808, MS L-202
LIVERMORE, CA 94551

LAWRENCE LIVERMORE NATIONAL LABORATORY
ATTN: TECHNICAL STAFF (PLS ROUTE)
PO BOX 808, MS L-195
LIVERMORE, CA 94551

LAWRENCE LIVERMORE NATIONAL LABORATORY
ATTN: TECHNICAL STAFF (PLS ROUTE)
PO BOX 808, MS L-205
LIVERMORE, CA 94551

THORNE LAY
UNIVERSITY OF CALIFORNIA, SANTA CRUZ
EARTH SCIENCES DEPARTMENT
EARTH & MARINE SCIENCE BUILDING
SANTA CRUZ, CA 95064

ANATOLI L. LEVSHIN
DEPARTMENT OF PHYSICS
UNIVERSITY OF COLORADO
CAMPUS BOX 390
BOULDER, CO 80309-0309

DONALD A. LINGER
DNA
6801 TELEGRAPH ROAD
ALEXANDRIA, VA 22310

LOS ALAMOS NATIONAL LABORATORY
ATTN: TECHNICAL STAFF (PLS ROUTE)
PO BOX 1663, MS F659
LOS ALAMOS, NM 87545

LOS ALAMOS NATIONAL LABORATORY
ATTN: TECHNICAL STAFF (PLS ROUTE)
PO BOX 1663, MS F665
LOS ALAMOS, NM 87545

LOS ALAMOS NATIONAL LABORATORY
ATTN: TECHNICAL STAFF (PLS ROUTE)
PO BOX 1663, MS D460
LOS ALAMOS, NM 87545

LOS ALAMOS NATIONAL LABORATORY
ATTN: TECHNICAL STAFF (PLS ROUTE)
PO BOX 1663, MS C335
LOS ALAMOS, NM 87545

GARY MCCARTOR
SOUTHERN METHODIST UNIVERSITY
DEPARTMENT OF PHYSICS
DALLAS, TX 75275-0395

KEITH MCLAUGHLIN
MAXWELL TECHNOLOGIES
P.O. BOX 23558
SAN DIEGO, CA 92123

BRIAN MITCHELL
DEPARTMENT OF EARTH & ATMOSPHERIC SCIENCES
ST. LOUIS UNIVERSITY
3507 LACLEDE AVENUE
ST. LOUIS, MO 63103

RICHARD MORROW
USACDA/IVI
320 21ST STREET, N.W.
WASHINGTON, DC 20451

JOHN MURPHY
MAXWELL TECHNOLOGIES
11800 SUNRISE VALLEY DRIVE SUITE 1212
RESTON, VA 22091

JAMES NI
NEW MEXICO STATE UNIVERSITY
DEPARTMENT OF PHYSICS
LAS CRUCES, NM 88003

JOHN ORCUTT
INSTITUTE OF GEOPHYSICS AND PLANETARY PHYSICS
UNIVERSITY OF CALIFORNIA, SAN DIEGO
LA JOLLA, CA 92093

PACIFIC NORTHWEST NATIONAL LABORATORY
ATTN: TECHNICAL STAFF (PLS ROUTE)
PO BOX 999, MS K6-48
RICHLAND, WA 99352

PACIFIC NORTHWEST NATIONAL LABORATORY
ATTN: TECHNICAL STAFF (PLS ROUTE)
PO BOX 999, MS K7-34
RICHLAND, WA 99352

PACIFIC NORTHWEST NATIONAL LABORATORY
ATTN: TECHNICAL STAFF (PLS ROUTE)
PO BOX 999, MS K6-40
RICHLAND, WA 99352

PACIFIC NORTHWEST NATIONAL LABORATORY
ATTN: TECHNICAL STAFF (PLS ROUTE)
PO BOX 999, MS K5-72
RICHLAND, WA 99352

PACIFIC NORTHWEST NATIONAL LABORATORY
ATTN: TECHNICAL STAFF (PLS ROUTE)
PO BOX 999, MS K5-12
RICHLAND, WA 99352

KEITH PRIESTLEY
DEPARTMENT OF EARTH SCIENCES
UNIVERSITY OF CAMBRIDGE
MADINGLEY RISE, MADINGLEY ROAD
CAMBRIDGE, CB3 0EZ UK

PAUL RICHARDS
COLUMBIA UNIVERSITY
LAMONT-DOHERTY EARTH OBSERVATORY
PALISADES, NY 10964

CHANDAN SAIKIA
WOODWARD-CLYDE FEDERAL SERVICES
566 EL DORADO ST., SUITE 100
PASADENA, CA 91101-2560

SANDIA NATIONAL LABORATORY
ATTN: TECHNICAL STAFF (PLS ROUTE)
DEPT. 6116
MS 0750, PO BOX 5800
ALBUQUERQUE, NM 87185-0750

SANDIA NATIONAL LABORATORY
ATTN: TECHNICAL STAFF (PLS ROUTE)
DEPT. 9311
MS 1159, PO BOX 5800
ALBUQUERQUE, NM 87185-1159

SANDIA NATIONAL LABORATORY
ATTN: TECHNICAL STAFF (PLS ROUTE)
DEPT. 5736
MS 0655, PO BOX 5800
ALBUQUERQUE, NM 87185-0655

THOMAS SERENO JR.
SCIENCE APPLICATIONS INTERNATIONAL
CORPORATION
10260 CAMPUS POINT DRIVE
SAN DIEGO, CA 92121

PACIFIC NORTHWEST NATIONAL LABORATORY
ATTN: TECHNICAL STAFF (PLS ROUTE)
PO BOX 999, MS K7-22
RICHLAND, WA 99352

PACIFIC NORTHWEST NATIONAL LABORATORY
ATTN: TECHNICAL STAFF (PLS ROUTE)
PO BOX 999, MS K6-84
RICHLAND, WA 99352

FRANK PILOTTE
HQ/AFTAC/TT
1030 S. HIGHWAY A1A
PATRICK AFB, FL 32925-3002

JAY PULLI
RADIX SYSTEMS, INC.
6 TAFT COURT
ROCKVILLE, MD 20850

DAVID RUSSELL
HQ AFTAC/TTR
1030 SOUTH HIGHWAY A1A
PATRICK AFB, FL 32925-3002

SANDIA NATIONAL LABORATORY
ATTN: TECHNICAL STAFF (PLS ROUTE)
DEPT. 5704
MS 0979, PO BOX 5800
ALBUQUERQUE, NM 87185-0979

SANDIA NATIONAL LABORATORY
ATTN: TECHNICAL STAFF (PLS ROUTE)
DEPT. 5791
MS 0567, PO BOX 5800
ALBUQUERQUE, NM 87185-0567

SANDIA NATIONAL LABORATORY
ATTN: TECHNICAL STAFF (PLS ROUTE)
DEPT. 5704
MS 0655, PO BOX 5800
ALBUQUERQUE, NM 87185-0655

SANDIA NATIONAL LABORATORY
ATTN: TECHNICAL STAFF (PLS ROUTE)
DEPT. 6116
MS 0750, PO BOX 5800
ALBUQUERQUE, NM 87185-0750

AVI SHAPIRA
SEISMOLOGY DIVISION
THE INSTITUTE FOR PETROLEUM RESEARCH AND
GEOPHYSICS
P.O.B. 2286, NOLON 58122 ISRAEL

ROBERT SHUMWAY
410 MRAK HALL
DIVISION OF STATISTICS
UNIVERSITY OF CALIFORNIA
DAVIS, CA 95616-8671

DAVID SIMPSON
IRIS
1616 N. FORT MEYER DRIVE
SUITE 1050
ARLINGTON, VA 22209

BRIAN SULLIVAN
BOSTON COLLEGE
INSITUTE FOR SPACE RESEARCH
140 COMMONWEALTH AVENUE
CHESTNUT HILL, MA 02167

NAFI TOKSOZ
EARTH RESOURCES LABORATORY, M.I.T.
42 CARLTON STREET, E34-440
CAMBRIDGE, MA 02142

GREG VAN DER VINK
IRIS
1616 N. FORT MEYER DRIVE
SUITE 1050
ARLINGTON, VA 22209

TERRY WALLACE
UNIVERSITY OF ARIZONA
DEPARTMENT OF GEOSCIENCES
BUILDING #77
TUCSON, AZ 85721

JAMES WHITCOMB
NSF
NSF/ISC OPERATIONS/EAR-785
4201 WILSON BLVD., ROOM 785
ARLINGTON, VA 22230

JIANG XIE
COLUMBIA UNIVERSITY
LAMONT DOHERTY EARTH OBSERVATORY
ROUTE 9W
PALISADES, NY 10964

OFFICE OF THE SECRETARY OF DEFENSE
DDR&E
WASHINGTON, DC 20330

TACTEC
BATTELLE MEMORIAL INSTITUTE
505 KING AVENUE
COLUMBUS, OH 43201 (FINAL REPORT)

MATTHEW SIBOL
ENSCO, INC.
445 PINEDA COURT
MELBOURNE, FL 32940

JEFFRY STEVENS
MAXWELL TECHNOLOGIES
P.O. BOX 23558
SAN DIEGO, CA 92123

DAVID THOMAS
ISEE
29100 AURORA ROAD
CLEVELAND, OH 44139

LAWRENCE TURNBULL
ACIS
DCI/ACIS
WASHINGTON, DC 20505

FRANK VERNON
UNIVERSITY OF CALIFORNIA, SAN DIEGO
SCRIPPS INSTITUTION OF OCEANOGRAPHY IGPP, 0225
9500 GILMAN DRIVE
LA JOLLA, CA 92093-0225

DANIEL WEILL
NSF
EAR-785
4201 WILSON BLVD., ROOM 785
ARLINGTON, VA 22230

RU SHAN WU
UNIVERSITY OF CALIFORNIA SANTA CRUZ
EARTH SCIENCES DEPT.
1156 HIGH STREET
SANTA CRUZ, CA 95064

JAMES E. ZOLLWEG
BOISE STATE UNIVERSITY
GEOSCIENCES DEPT.
1910 UNIVERSITY DRIVE
BOISE, ID 83725

DEFENSE TECHNICAL INFORMATION CENTER
8725 JOHN J. KINGMAN ROAD
FT BELVOIR, VA 22060-6218 (2 COPIES)

PHILLIPS LABORATORY
ATTN: XPG
29 RANDOLPH ROAD
HANSCOM AFB, MA 01731-3010

PHILLIPS LABORATORY
ATTN: GPE
29 RANDOLPH ROAD
HANSCOM AFB, MA 01731-3010

PHILLIPS LABORATORY
ATTN: TSML
5 WRIGHT STREET
HANSCOM AFB, MA 01731-3004

PHILLIPS LABORATORY
ATTN: PL/SUL
3550 ABERDEEN AVE SE
KIRTLAND, NM 87117-5776 (2 COPIES)